
Electronic Thesis and Dissertation Repository

6-26-2015 12:00 AM

Using Ion Mobility Spectrometry to Study Protein Conformations in the Gas Phase

Yu Sun

The University of Western Ontario

Supervisor

Lars Konermann

The University of Western Ontario

Graduate Program in Chemistry

A thesis submitted in partial fulfillment of the requirements for the degree in Master of Science

© Yu Sun 2015

Follow this and additional works at: <https://ir.lib.uwo.ca/etd>

 Part of the [Analytical Chemistry Commons](#)

Recommended Citation

Sun, Yu, "Using Ion Mobility Spectrometry to Study Protein Conformations in the Gas Phase" (2015).

Electronic Thesis and Dissertation Repository. 2911.

<https://ir.lib.uwo.ca/etd/2911>

This Dissertation/Thesis is brought to you for free and open access by Scholarship@Western. It has been accepted for inclusion in Electronic Thesis and Dissertation Repository by an authorized administrator of Scholarship@Western. For more information, please contact wlsadmin@uwo.ca.

Using Ion Mobility Spectrometry to Study Protein Conformations in the Gas Phase

(Thesis format: Integrated-Article)

by

Yu Sun

Graduate Program in Chemistry

A thesis submitted in partial fulfillment
of the requirements for the degree of
Master of Science

The School of Graduate and Postdoctoral Studies
The University of Western Ontario
London, Ontario, Canada

© Yu Sun 2015

Abstract

The question whether electrosprayed protein ions retain solution-like conformations remains a matter of debate. One way to address this issue involves comparisons of collision cross sections (Ω) measured by travelling wave ion mobility spectrometry (TWIMS) with Ω values calculated for model structures. It is often implied that nanoESI is more conducive for the retention of solution structure than regular ESI. Focusing on four different proteins we demonstrated that Ω values and collisional unfolding profiles are virtually indistinguishable under both conditions. Calibration can be challenging because differences in the extent of collisional activation for TWIMS and drift tube calibrant data may lead to ambiguous peak assignments. We illustrated that these difficulties can be circumvented by employing collisionally heated calibrant ions. For interpreting experimental Ω values we generated gas phase model structures using molecular dynamics (MD) simulations, instead of solely relying on crystallographic data. Overall, our data are consistent with the view that exposure of native proteins to electrospray conditions can generate kinetically trapped ions that retain solution-like structures on the millisecond time scale of IMS experiments.

Keywords: mass spectrometry, travelling-wave ion mobility spectrometry, collision cross section, calibration, molecular dynamics simulations

Statement of Co-Authorship

The work in Chapters 2 and 3 were submitted in the following articles:

Sun Y, Vahidi S, Sowole MA, McAllister RG, and Konermann L (2015) Protein Structural Studies by Traveling Wave Ion Mobility Spectrometry: A Critical Look at Calibration, Electrospray Sources, and Molecular Dynamics Models. *Analyst*. (Submitted)

The original draft of this manuscript was prepared by the author. Subsequent revisions was performed by the author and Dr. Lars Konermann and other co-authors. All experimental work was performed by the author under the supervision of Dr. Lars Konermann. Molecular dynamics simulations in chapter 3 were developed by Dr. Lars Konermann and Robert McAllister of our group.

Acknowledgement

First of all, I wish to express my sincere appreciation to my supervisor Dr. Lars Konermann. He has offered his generous patience and encouragement from the first day I came to the lab. My gratitude to his support and inspiration is more than I could say. His excellent expertise guided me to the amazing world of proteins and mass spectrometry. I benefit from his passion for the research and conscientiousness for the work. These outstanding characters would stimulate me to further efforts. I have really enjoyed my studies in Konermann's lab, and this experience would be the most memorable time in my life.

I want to thank my committee members and examiners: Dr. Gary Shaw, Dr. François Lagugné-Labarthe, Dr. Patrick O'Donoghue, Dr. Zhifeng Ding and Dr. Ajay Ray.

I also want to take this opportunity to thank all the past and present group members for their support and suggestions. Thanks to Yue, his warm encouragement made me feel more comfortable about the unknown environment and made me start my experiments more easily. Thanks to Ming, Haidy and Robert, they shared their friendliness and their outstanding ideas about the research with me, which enlightened me a lot about my study. Thanks to Dupe, she always likes to explain my questions and give me many wonderful suggestions. A special thank to Siavash, who is another mentor to me. He taught me how to use the instruments hand by hand and he likes to provide any useful idea to help me with the challenges. Thanks as well to Antony, Stephanie, Courtney, Danielle, Lauren and Samuel.

Last but not least, I want to thank my beloved family and my friends. Thanks for their love, support and accompany.

Table of Contents

Abstract.....	i
Statement of Co-Authorship	ii
Acknowledgement	iii
List of Tables	vii
List of Figures.....	viii
List of Symbols and Abbreviations	x
Chapter 1 - Introduction	1
1.1 Protein Structure and Function.....	1
1.1.1 General Considerations	1
1.1.2 Protein Folding.....	1
1.1.3 Techniques for Studying Proteins.....	2
1.2 Mass Spectrometry	5
1.2.1 Ionization Techniques	5
1.2.2 Mass Analyzer	14
1.3 Ion Mobility Spectrometry (IMS)	21
1.3.1 Drift Tube Ion Mobility Spectrometry (DTIMS).....	21

1.3.2	Drift Field and Resolution	24
1.3.3	Collision Cross Section (CCS).....	25
1.3.4	Travelling Wave Ion Mobility Spectrometry (TWIMS).....	28
1.4	Scope of this Thesis.....	32
1.5	References	34
Chapter 2 - Calibration Issues in TWIMS		45
2.1	Introduction	45
2.2	Experimental	47
2.2.1	Sample Preparation	47
2.2.2	Instrument Settings	48
2.2.3	TWIMS Calibration	49
2.3	Results and Discussion.....	51
2.4	Conclusion.....	57
2.5	References	58
Chapter 3 - Protein Structural Studies by TWIMS: A Critical Look at ESI Sources and Molecular Dynamics Models.....		62
3.1	Introduction	62

3.2	Experimental	65
3.2.1	Sample Preparation	65
3.2.2	Instrument Settings	65
3.2.3	Molecular Dynamics Simulations.....	66
3.3	Results and Discussion.....	68
3.3.1	Instrument-to-Instrument Reproducibility	68
3.3.2	TWIMS of Native Proteins Using Regular ESI and nanoESI	70
3.3.3	X-ray Structure and MD Conformation.....	76
3.3.4	Comparison of TWIMS Data with MD-Derived and Crystallographic Ω_{EHSS} Values	82
3.4	Conclusions	83
3.5	References	86
Chapter 4 - Conclusions		92
4.1	Conclusions and Future Work.....	92
4.2	References	95
Curriculum Vitae		97

List of Tables

Table 1.....	50
--------------	----

List of Figures

Figure 1-1 Schematic Depiction of an ESI Source	8
Figure 1-2 Mechanisms of Electrospray Ionization.	11
Figure 1-3 Optical Microscopy Image of a Nanospray Capillary before breaking.	13
Figure 1-4 Schematic Description of Quadrupole Operation.	17
Figure 1-5 Schematic layout of mass spectrometer (Synapt G1) used in this work.	20
Figure 1-6 Drift Time IMS Separator (DTIMS).	23
Figure 1-7 An Approximate Schematic Diagram of Collision Cross Section (CCS).	27
Figure 1-8 Travelling Wave Ion Guide (TWIG).	29
Figure 1-9 Travelling Wave IMS Separator.....	31
Figure 2-1 Effects of sample cone voltage on the TWIMS profiles of the Ubq/Cyt/aMb calibrant mix.....	52
Figure 2-2 Partial ESI mass spectra, showing the appearance of CID.	53
Figure 2-3 Calibration plots for the Ubq/Cyt/aMb calibrant mix.....	56
Figure 3-1 TWIMS profile for Cyt 8+ at pH 3.	69
Figure 3-2 Mass spectra of four proteins under gentle conditions.....	71

Figure 3-3 Calibrated TWIMS data for four proteins under native condition.....	72
Figure 3-4 Calibrated TWIMS profiles for the ion species noted along the top.	74
Figure 3-5 Average collision cross sections Ω_{av} as a function of cone voltage.....	75
Figure 3-6 Root mean square deviation (RMSD) of the four model proteins.	79
Figure 3-7. Radius of gyration (R_g) of four proteins.....	80
Figure 3-8 Comparison of crystal structures (red) and MD simulation results for t = 40 ns (blue).....	81

List of Symbols and Abbreviations

aMb – apo-myoglobin

$a(r_i)$ – acceleration

ADH – alcohol dehydrogenase

CCS – collision cross section

CD – circular dichroism

CEM – chain ejection mechanism

CI – chemical ionization

CID – collisional-induced dissociation

CRM – charged-residue mechanism

Cyt – cytochrome c

Cyro-EM – cyro-electron microscopy

DC – direct current

DTIMS – drift tube ion mobility spectrometry

E – electric field

E_k – kinetic energy

E_p – potential energy

EI – electron impact

EHSS – hard sphere scattering method

ESI – electrospray ionization

FT-ICR – fourier transform ion cyclotron resonance

FWHM – full width at half maximum

ΔG – difference in Gibb's free energy

hMb – holo-myoglobin

Hb – hemoglobin

HDX – hydrogen-deuterium exchange

ΔH – enthalpy change

IEM – ion evaporation mechanism

IMS – ion mobility spectrometry

k_0 – reduced mobility

k_B – Boltzmann's constant

K – ion mobility

L – length of drift tube

MALDI – matrix-assisted laser desorption/ionization

MD – molecular dynamics

MS – mass spectrometry

nanoESI – nanoelectrospray ionization

N – native conformation

NMR – nuclear magnetic resonance

PA – projection approximation

PD – plasma desorption

PSA – projected superposition approximation

r_i – coordinate

RF – radio frequency

RMSD – root mean square deviation

R_g – radius of gyration

γ – surface tension

ΔS – entropy change

t_d – drift time

TM – trajectory method

TOF – time of flight

TWIG – travelling wave ion guide

TWIMS – travelling wave ion mobility spectrometry

U – unfolded conformation

Ubq – ubiquitin

UV-Vis – ultraviolet-visible

μ – reduced mass

V_d – drift velocity

$V(r_i)$ – force field

z_R – charge at Rayleigh limit

Ω – collision cross section value

Chapter 1 - Introduction

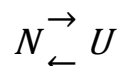
1.1 Protein Structure and Function

1.1.1 General Considerations

Proteins are important biopolymers that carry out a variety of cellular functions. They catalyze metabolic reactions, participate in cellular communication or cellular defense.¹ These functions are all attributed to the unique structures of proteins. Most proteins consist of 20 amino acids which are usually linked by covalent bonds. Primary structure refers to the sequence of amino acids. It determines the native 3D structure of proteins. The higher order structure in proteins is based to a large extent on intramolecular hydrogen bonding between the amide H and CO groups of the backbone. α -helices and β -sheets are the most common motifs of secondary structure. Hydrophobic interactions and salt bridges between charged side chains give rise to the tertiary structure. Ultimately, two or more protein chains can assemble to form multisubunit complexes, thus giving rise to be the highest level of molecular organization, quaternary structure.

1.1.2 Protein Folding

Proteins usually function when they are folded into unique stable structures. Considering a simple two-state equilibrium between the native state (N) and the unfolded state (U):



the Gibb's free energy difference can be expressed as

$$\Delta G = \Delta H - T\Delta S \quad (1.1)$$

There are many factors contributing to enthalpic (ΔH) and entropic (ΔS) terms. Intramolecular hydrogen bonds, and hydrogen bonds between proteins and solvent are major contributors to ΔH .²⁻³ The hydrophobic effect gives rise to entropic changes, commonly attributed to the "iceberg water" model.⁴⁻⁵ In native proteins, hydrophobic residues are buried in the core. This allows minimizing the shell water so that entropy is maximized. Anfinsen's work on the folding of RNase A earned him the Chemistry Nobel Prize in 1972.⁶ His work indicated that N is the conformation with the lowest free energy. Anfinsen also demonstrated that the amino acid sequence determines the native 3D structure of protein.

Why is the protein folding problem so important? Deciphering the folding problem is key to predict the 3D structures of proteins from their sequences. Protein structures determine cellular functions. Knowledge of protein structures therefore gives insight into the biological processes at the molecular level. Besides, understanding the folding process helps to design protein drugs. It also helps to find ways of preventing misfolding diseases.⁷⁻⁸ Another important aspect is the design and synthesis of *de-novo* proteins. For example, we can initiate changes for the target sequence to make enzymes catalysing non-natural reactions.⁹

1.1.3 Techniques for Studying Proteins

Optical techniques are widely used for studying proteins. Common examples include Ultraviolet-visible (UV-Vis) absorption spectroscopy, circular dichroism (CD) spectroscopy and fluorescence spectroscopy. These techniques monitor the transition of electrons between

molecular orbitals. The benefit of optical spectroscopy lies in the ability to function under physiological conditions without chemical modifications. They mainly provide conformational information on a global scale. In UV-Vis spectroscopy, conjugated systems absorb light. The absorbance is determined by the absorption coefficient and concentration of the sample.¹⁰ In addition to concentration measurement, conformational change of proteins can be detected. For example, the heme present in some proteins is a prosthetic group that has strong electronic absorption bands that depend on its metal oxidation state, ligation, and chromophore environment.¹¹ The conformation of heme-bound proteins depends on the ligation state of heme iron and the variants in the structure and the spin state of iron.¹² In this way, the conformational changes can be detected by the appearance of a band shift in UV-Vis spectroscopy.

CD spectroscopy utilizes differential absorption between left- and right-polarized light by chiral molecules. Different secondary structures give rise to distinct signals such as α -helix, β -sheet and random coil. However, the information provided by CD spectroscopy does not provide a lot of details, therefore this method is often used to complement other techniques.¹³

Fluorescence is another popular spectroscopic technique that is based on the emission of light when molecules return from an excited state to the ground state. Tryptophan, as an indole chromophore, is highly sensitive to the environment, so that it can report on conformational changes and intermolecular interactions.¹⁴

X-ray crystallography is a critically important technique for studying protein 3D structures. Proteins cannot be observed directly by optical microscopy because of their small sizes. However, the atomic distance within proteins ($\sim 1.5 \text{ \AA}$) is similar to the wavelength of X-rays.

In an ordered crystal, the unit cell is defined as the smallest volume element. The protein molecules are aligned in a repeating array of these unit cells which are arranged along the cell axes. The crystal planes of atoms, formed by the arrays produce diffraction patterns when exposed to X-ray radiation.¹⁵ Crystallography has made great contributions as it yielded thousands of protein crystal structures deposited in the Protein Data Bank. However, the growth of protein crystals is still a big challenge, especially for membrane proteins. Additionally, there is the problem that this method does not usually provide information on protein dynamics.¹⁶ In recent years, crystallographic techniques have been developed for studying enzyme dynamics by targeting transient intermediate states.¹⁷⁻¹⁸ Nonetheless information on large-scale dynamic events is still difficult to obtain.

Nuclear magnetic resonance (NMR) spectroscopy has evolved to become one of the most powerful tools to study protein structure and dynamics. In a magnetic field, the spin energy of nuclei is split into two levels. Upon application of electromagnetic radiation, each nucleus can resonate at a specific frequency which is highly dependent on the local environment. Thus, NMR spectroscopy can provide structural and dynamic information. In terms of dynamics, NMR can also cooperate with hydrogen-deuterium exchange (HDX) experiment. If the protein is exposed to heavy water, the conversion of NH to ND causes the disappearance of the corresponding peaks, due to the invisibility of deuterium in NMR.¹⁹⁻²⁰ Nevertheless, for large proteins, resonance overlap and peak broadening become significant issues. The upper size limit is around 40 kDa.²¹ In addition, NMR experiments require milimolar (or high micromolar) concentrations which increases the possibility of aggregation and misfolding.

Cryo-electron microscopy (cryo-EM) provides structural information as well. Three-dimensional data can be obtained by combining different projections of molecule and

reconstruction.²² However, cyro-EM suffers from low resolution.²³ Cryo-EM is often combined with other high resolution techniques to provide structures of large sub-cellular assemblies.

1.2 Mass Spectrometry

Mass spectrometry (MS) has been introduced over a century ago.²⁴ Nowadays it has become one of the most significant techniques used to examine the structures, interactions, and dynamics of proteins. In principle, MS measures mass to charge ratio (m/z) of analyte ions in vacuum. Thus, each mass spectrometer typically comprises an ion source and a mass analyzer.

1.2.1 Ionization Techniques

The basic principle of MS is to utilize the effects of electric and/or magnetic fields on charged particles, so all the neutral molecules have to be ionized before they enter the analyzer. Different ionization techniques can be applied, such as electron impact (EI), chemical ionization (CI), plasma desorption (PD) and matrix-assisted laser desorption/ionization (MALDI).²⁵ However, ionization often gives rise to dissociation of analyte molecules yielding abundant fragment ions. For example, EI induces rupture of covalent bonds. MALDI was developed by *Tanaka* and he was awarded the Nobel Prize in Chemistry in 2002.²⁶⁻²⁷ Briefly, in MALDI, a sample is spotted on a matrix. After drying, the sample is brought into the gas phase where a laser beam hits the sample-matrix crystal. The matrix absorbs the laser energy, and desorption and ionization occur subsequently.²⁸ MALDI achieves superior sensitivity in the high mass range and it is tolerant to salt.²⁹ On the other hand, MALDI generally produces

singly charged ions which is not quite adequate for many application such as top-down tandem MS.

Electrospray Ionization (ESI)

ESI was first coupled with MS in the 1980s by Fenn.³⁰ It is regarded as a “soft” ionization technique which can produce multiply charged ions. The term “soft” refers to minimum internal energy transmitted to the analytes during the ionization process.³¹ The softness property is necessary when detecting intact proteins with the goal of preserving solution phase structures.

The principle of ESI (Figure 1-1) is to dissolve protein samples in solution which is injected into a narrow (~100 μm) metal capillary. Upon application of a high voltage (2-3 kV), positive and negative electrolyte ions will move under the influence of the electric field. Electrons in solution move away from the capillary tip. Charge balancing redox reaction takes place including $\text{H}_2\text{O} \rightarrow 2\text{H}^+ + 2\text{e}^- + \frac{1}{2} \text{O}_2$. Then the positively charged solution is distorted into a Taylor cone.³² If the applied field is sufficiently high, the cone tip becomes unstable so that a fine mist of charged droplets is released from the cone. These initial droplets have radii in the micrometer range. They are positively charged due to excess ions (H^+ , NH_4^+ , Na^+ and K^+), and they are accelerated by electric potential difference between the capillary and the sampling cone. During the process of acceleration, solvent evaporates rapidly under the influence of heating and nebulizer gas. As the droplets shrink, their charge to volume ratio increases until Coulombic repulsion overcomes surface tension.³³ Under this circumstance, the number of charges z_R is given by Rayleigh limit:³⁴

$$z_R = \frac{8\pi}{e} \sqrt{\varepsilon_0 \gamma R^3} \quad (1.2),$$

where R is the droplet radius, ϵ_0 is the vacuum permittivity, and γ is the surface tension. Droplet fission occurs at the Rayleigh limit, producing smaller offspring droplets. After several evaporation/ fission cycles, multiply protonated protein ions are released into the gas phase.

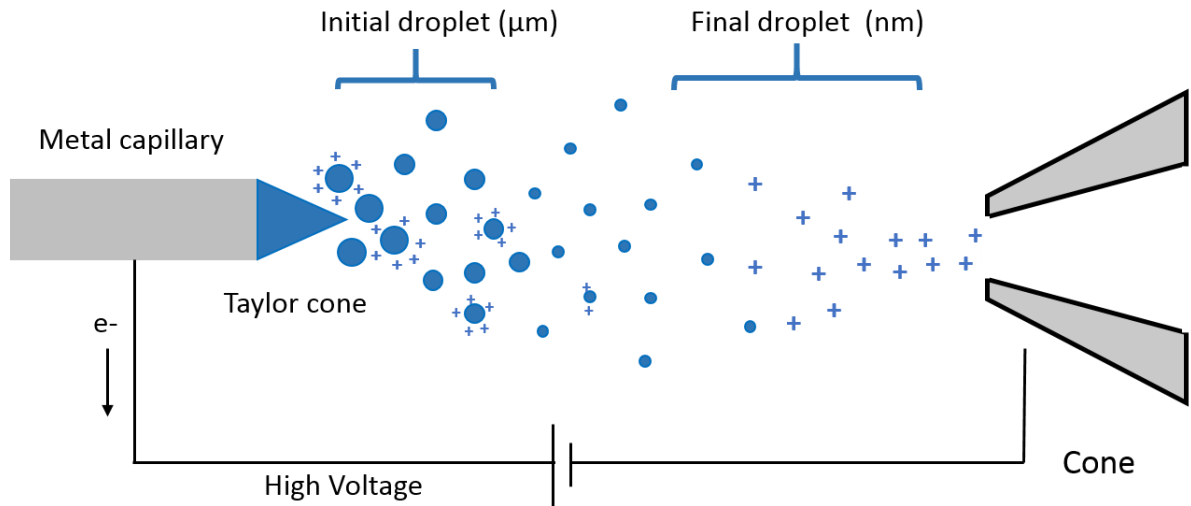


Figure 1-1 Schematic Depiction of an ESI Source

Upon the application of a high voltage, the positively charged ions accumulate at the metal capillary. Then the positive charged solution is distorted into a Taylor cone and the tip releases a fine mist of charged droplets. Under the effect of Coulombic repulsion and surface tension, the initial droplets experience evaporation/fission cycles to produce offspring droplets, and ultimately analyte ions.

The mechanisms by which gaseous ions are formed during ESI is still in dispute. The two most favored mechanisms are the charged-residue mechanism (CRM)³⁵ and ion-evaporation mechanism (IEM)³⁶. In the IEM, it is believed that the charge density becomes sufficiently high due to the large electric field at the surface of droplet, so that ions which carry most of charges are ejected directly out of the nanodroplets.³⁷⁻⁴⁰ This model was proved by experiments that explains how metal ions are formed during ESI.⁴¹⁻⁴² On the other hand, native folded proteins are considered to follow the CRM (Figure 1-2 a.). The idea is that after a succession of fissions, the droplets would be so small that finally contain only one solute protein. As the last solvent evaporates from the nanodroplets, the excess charges are retained on proteins so that droplets become gas-phase ions.^{35, 43} During the shrinkage, the charges on the molecules are limited by the Rayleigh charge.⁴⁴ Experimental work in support of the CRM for globular proteins has shown that analyte ions are composed of $[M + z_R H]^{z_R+}$, where z_R is the Rayleigh charge of protein-sized water droplets.⁴⁴⁻⁴⁶ Computational studies have also confirmed that globular analytes are trapped deep within the droplet due to the hydration of hydrophilic parts on proteins, which is not favored to IEM.⁴⁷⁻⁴⁹

However, the CRM is not always suitable for all protein ions. We know that in neutral solution, most proteins adopt compact folded conformation, which consist of a hydrophobic core and hydrophilic exterior. Most nonpolar residues are buried in the core, whereas many polar and charged residues are pointing to the outside.⁵⁰⁻⁵¹ Once the protein is placed in a denatured environment, they tend to be denatured and hydrophobic interior becomes exposed to the solvent.⁵²⁻⁵⁵ In this case, protein ions are thought to be released via a different type of process, referred to as chain ejection model (CEM) (Figure 1-2 b.).^{47, 56} Molecular dynamics simulations indicated that compact proteins remain inside the Rayleigh charged nanodroplet.⁴⁷

For unfolded proteins, exposed hydrophobic sites drive the analyte to the droplet surface due to unfavorable water interaction.⁵⁷ In analogy with the IEM, one chain terminus is expelled into the gas phase, and then followed by sequential ejection of the remaining chain under the effect of Coulomb repulsion between positively charged side chains and charges on the droplet. In conclusion, CRM and CEM apply to the ESI process of folded and unfolded proteins, respectively. The IEM explains how low molecular weight ions are formed during ESI.

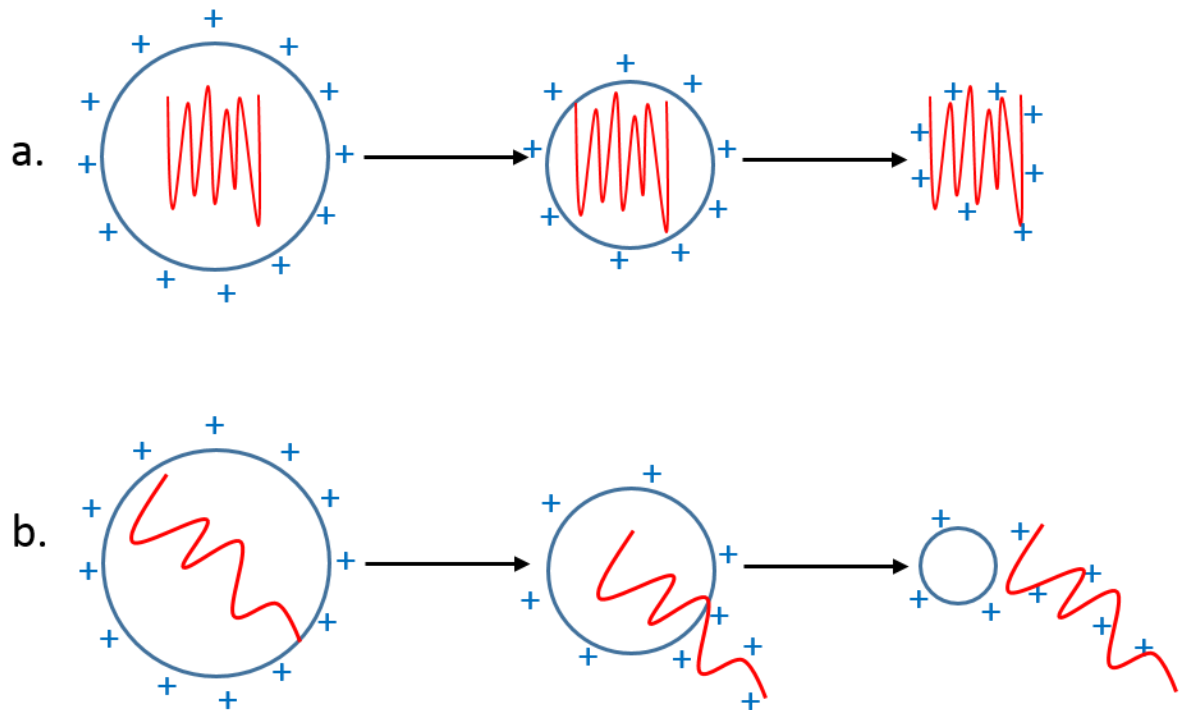


Figure 1-2 Mechanisms of Electrospray Ionization.

a. Charged-residue mechanism (CRM): native proteins are retained in the droplets during the shrinkage/fission process. As the last solvent evaporates, excess charges remain on the protein.

b. Chain ejection model (CEM): unfolded proteins are following the CEM. One chain terminus is expelled into the gas phase because of the hydrophobic effect. The remaining chains are then ejected under the effect of Coulomb repulsion between positively charged side chains and charges on the droplet.

Nanoelectrospray Ionization (Nano ESI)

In terms of ESI techniques, there are two options existing to convert solution phase analytes to gaseous ions. Regular ESI operates at the flow rate in the $\mu\text{L}/\text{min}$ range, using a metal emitter capillary.^{30, 58} NanoESI operates with a much smaller spray capillary (Figure 1-3), giving rise to flow rate of less than 100 nL/min.⁵⁹ NanoESI was first proposed by Wilm, Mann and coworkers.⁶⁰⁻⁶¹ They pointed out that achieving a low flow rate can be beneficial in many ways. The initial droplets from nanoESI have diameters of less than 200 nm due to the smaller capillary orifice, which are about 100 to 1000 times smaller than in regular ESI.⁶⁰ In the aspect of operation, the potential applied on the capillary is around 0.5-1.5 kV, which is significantly lower than regular ESI, although it always needs an auxiliary pressure to initiate and maintain a steady flow of solution.⁶² Considering such low flow rate and small volume of initial droplets, nanoESI can be associated with several advantages. First of all, less sample is required. Only 1-2 μL of sample is loaded directly into the gold-coated glass capillaries.⁶³ Solution is drawn through the capillary without a conventional syringe pump. Secondly, ionization efficiency is improved, which is supported by a series of experiments.⁶⁴⁻⁶⁷ The ionization efficiency can be characterized as the ratio between the number of detected analyte molecules and the total number of ions in the solution delivered to the ionization source.⁶⁸ It is commonly accepted that fission events of the initial droplets lead to lose of a relatively large percentage of charges and a relatively small percentage of mass.⁶⁹ Thus, smaller initial droplets produced by nanoESI experience less fission cycles and provide larger fraction of the analyte molecules to become available for analysis.⁷⁰

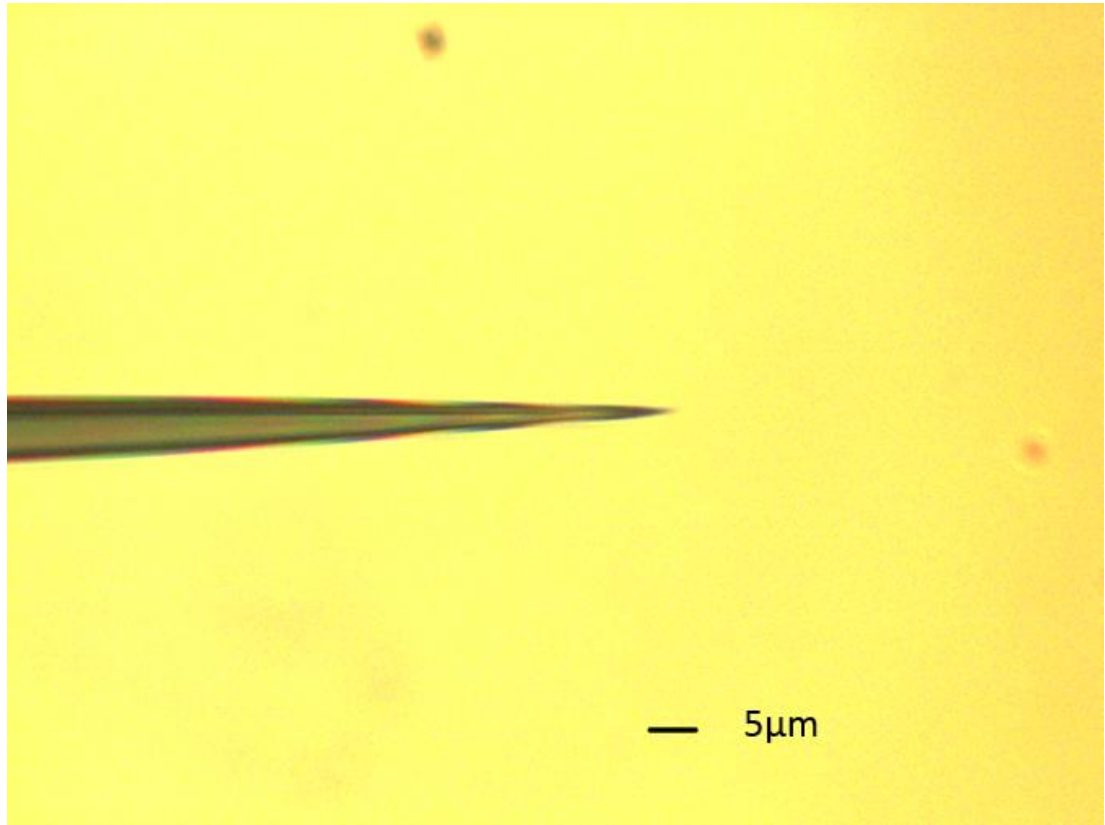


Figure 1-3 Optical Microscopy Image of a Nanospray Capillary before breaking.

The diameter of the capillary tip is much less than 1µm.

Additionally, nanoESI is believed to have a higher salt tolerance, at least an order of magnitude better than regular ESI.⁷¹⁻⁷² With both techniques, evaporation steadily increases the concentration of both analyte and non-volatile salt contaminants in the droplets. NanoESI emits initial droplets with lower size and higher charge density, which results in a lower number of fission events. In other words, the Rayleigh charging droplets form earlier without extensive solvent evaporation. Therefore, the extent of salt enrichment is minimized.^{62, 71} However, nanoESI also suffers from some drawbacks. It tends to be less robust in terms of signal stability and reproducibility than regular ESI.⁷³⁻⁷⁴

1.2.2 Mass Analyzer

Once the protein ions are produced by ESI and transferred into vacuum, they are ready to be separated and detected by mass analysis techniques. Mass spectrometer measures mass to charge ratio, which is given by

$$m/z = \frac{[m+zH]}{z} \quad (1.3)$$

assuming that the entire charge is due to excess protons. When the sprayed proteins contain salt contaminants, the net charge has to take salt ions into account. For example, if Na⁺ is present in the protein, mass to charge ratio is considered as

$$m/z = \frac{[m+(z-i)H+iNa]}{z} \quad (1.4)$$

where *i* refers to the number of sodium ions attached to the protein. Some issues have to be considered for a high quality mass measurements. First of all is the mass range of the mass analyzer. For instance, MALDI typically produces singly or low charge state ions. Thus, it

requires a mass analyzer with an extended m/z range. ESI, on the other hand, usually provides multiply charged ions, so that it would be compatible with many types of mass analyzers. Another important aspect is the sensitivity. High sensitivity allows mass analyzers to detect analytes even at low concentration. The third key feature is the resolution. Mass resolution refers to the minimal difference between two m/z values present in the spectrum that allows a clear distinction. The classical definition of resolution power R is given by:

$$R = \frac{M}{\Delta M} \quad (1.5)$$

where M is the m/z value of a particular ion peak. Historically, according to valley definition, ΔM is the width of a specified peak at 5% of its height, so that the valley between the two equal intensity peaks is 10% of the maximum intensity. More recently, another definition is based on the peak width, where ΔM is the full width at half maximum (FWHM) for each respective peak.

Quadrupoles

Quadrupoles represent one of the most common devices used in MS. They can be used for ion storage in which gaseous ions can be confined for a period of time.⁷⁵ It can also function as ion guide or mass filter. Single quadrupoles were introduced as mass filter for studying proteins.⁷⁶⁻⁷⁸ However, the limitation lies in the narrow m/z range, which is limited to 4000. MS/MS experiments can be carried out if three quadrupoles are arranged in series, the so-called triple quadrupoles.⁷⁹⁻⁸⁰ The first quadrupole is set for selecting precursor ions, while the second one is used as a collision cell that gives rise to collision induced dissociation. The third quadrupole works as a mass analyzer that transmits a certain m/z from fragment ion spectrum.

A quadrupole (Figure 1-4) is composed of two pairs of charged parallel cylindrical metal rods, one pair positively and the other negatively charged. These four rods are connected diagonally, so that the same charges are facing each other. Upon the application of a radio frequency (RF) voltage, ions can pass through because of the potential gradient between the inlet and outlet of the quadrupoles. A direct current voltage (DC) can be superimposed onto the RF voltage to implement mass filter operation. The DC voltage provides a stable trajectory for only one m/z value, while a slightly increase or decrease of m/z value will result in an unstable trajectory so that they will collide with the rods and never reach the detector. If DC voltage is tuned to zero which is regarded as an “RF only” mode, the quadrupoles act as an ion guide instead of an ion filter. It allows all the ions traverse through but confines them in the center, avoiding radial diffusion.⁸¹

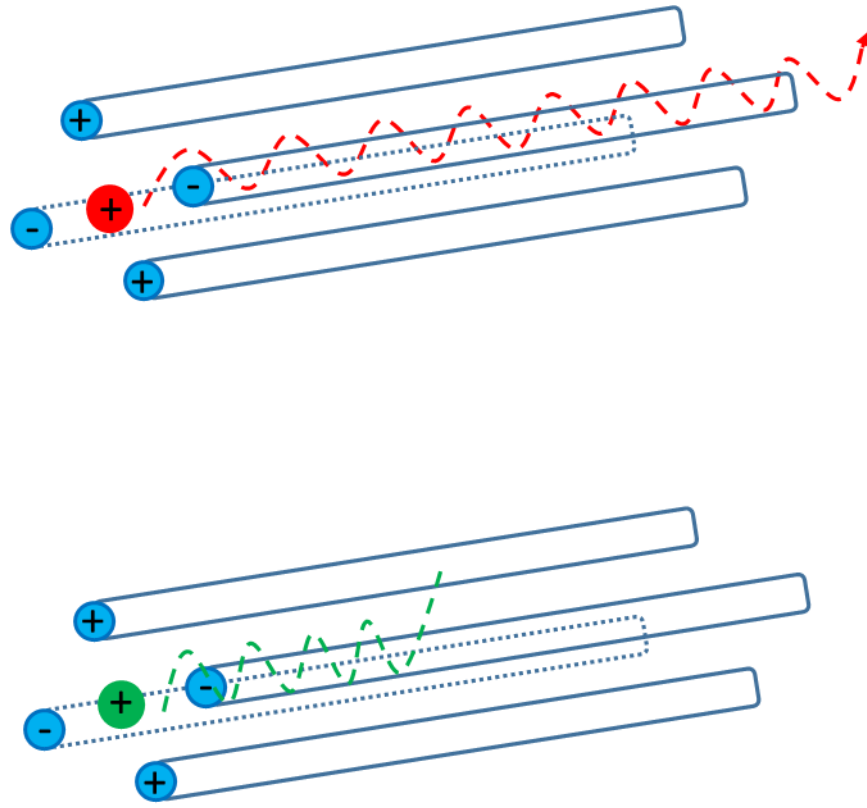


Figure 1-4 Schematic Description of Quadrupole Operation.

For a certain combination of DC/RF voltages, only ions of a certain m/z values (red line) can pass through the quadrupole. Other m/z values have unstable trajectories (green line).

Time-of-Flight (TOF) Mass Analyzer

The time-of-flight concept was introduced half a century ago.⁸² It is used more commonly than the quadrupole as a mass analyzer due to its wider mass range. The principle of TOF operation is based on the conversion of potential energy to kinetic energy. The ions are accelerated into a field free flight tube. In the pusher region, the potential energy E_p is converted to kinetic energy E_k ,

$$E_p = E_k$$

$$zeU = \frac{1}{2} mv^2 \quad (1.6)$$

where U refers to the acceleration voltage, m refers to the mass of the ion, and v is the velocity of the ion. The time (t) that ions spend to reach the detector can be described as:

$$zeU = \frac{1}{2} m \left(\frac{d}{t}\right)^2$$

$$t = \frac{d}{\sqrt{2eU}} \sqrt{\frac{m}{z}} \quad (1.7)$$

where d is the length of the flight tube. $\frac{d}{\sqrt{2eU}}$ is independent of the analyte, such that t only depends on m/z . The ionic signal intensity in the mass spectrum is a function of the arrival time. However, the simple approach described above gives poor mass resolution due to significant spread of ions. To improve the performance of the mass analyzer, orthogonal acceleration has been applied.⁸³⁻⁸⁴ This orthogonal version can reduce the initial velocity distribution along the TOF axis, so that ions are focused in an ion beam. Another “correction” for the initial energy is using a reflectron, which can be considered as a series of potential gradients.⁸⁵ When two

ions that have identical mass and charge first enter the TOF tube, they are accelerated perpendicularly. However, slight deviations in velocity cause the ions to arrive at the detector at different times, which decreases the resolution. Upon the setting of reflectron, the faster ion will penetrate deeper into the decelerating region so that it takes longer to be reflected towards the detector. The slower ion reaches the reflectron later but its trajectory path is shorter. In this way, the velocity deviation can be corrected and two ions with the same m/z will reach the detector at the same time.

Other Mass Analyzers

There are also other types of mass analyzers, such as Fourier Transform Ion Cyclotron Resonance (FT-ICR) MS and Orbitrap MS, which employ different mechanisms from that in TOF.⁸⁶⁻⁸⁹ FT-ICR MS is using a magnetic field to force ions into a cyclotron motion. The measurement of m/z is based on the cyclotron frequency. In Orbitrap MS, ions are placed in an electrostatic field. Under the influence of a central cylindrical electrode, ions orbit with an oscillate frequency which is related to m/z .⁸⁸ These two new types of mass analyzers not only widen the m/z range, but also significantly increase the resolution to 10^5 and beyond.⁹⁰

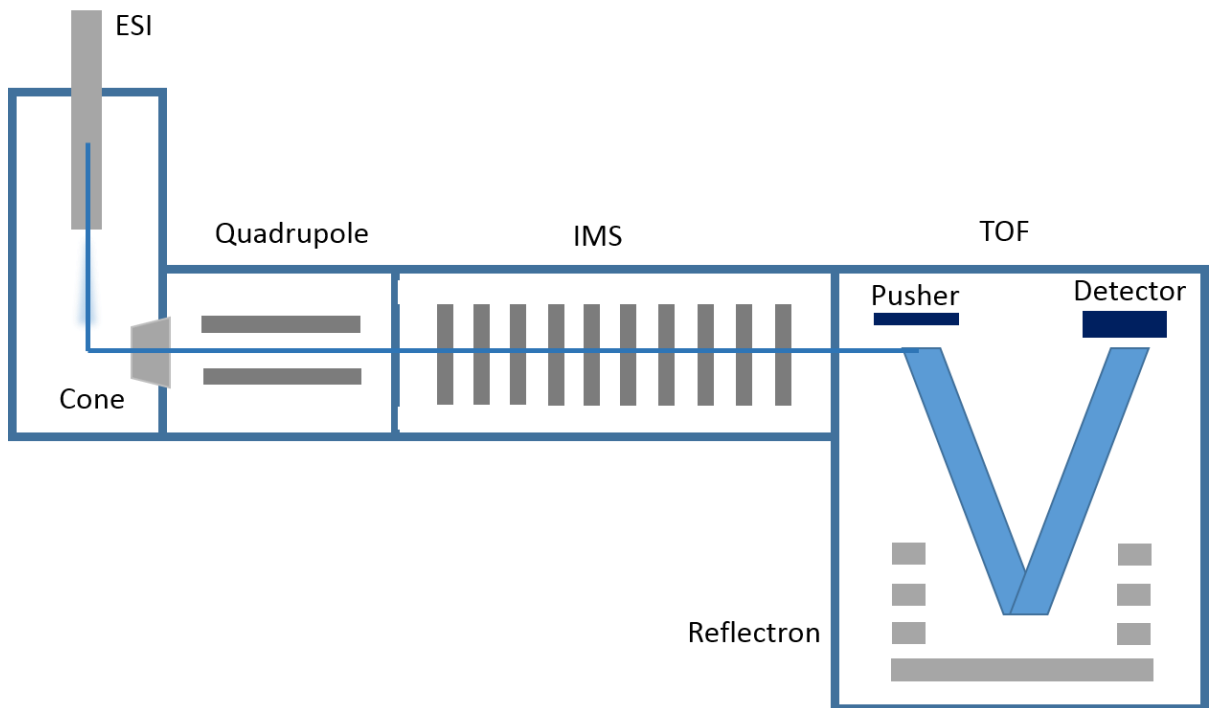


Figure 1-5 Schematic layout of mass spectrometer (Synapt G1) used in this work.

High voltage is applied on the capillary. From capillary voltage to trap bias downstream, the potential is decreasing. An orthogonal TOF with reflectron is used as mass analyzer.

1.3 Ion Mobility Spectrometry (IMS)

The advent of mass spectrometry provides an exciting opportunity to study gaseous protein ions. However, X-ray crystallography, NMR spectroscopy, and cryo-EM are only applicable in the condensed phase. Assisting MS for resolving images of solvent-free biomolecules, many spectroscopic tools are used, in addition to gas phase H/D exchange,⁹¹⁻⁹⁴ and computer simulations.⁹⁵⁻⁹⁷ Ion mobility spectrometry (IMS) has been combined with mass spectrometry (IMS-MS) to investigate the conformational properties of biomolecules in the gas phase.⁹⁸⁻¹⁰¹ *Clemmer*, and *Jarrold* were the first to resolve different protein ion structures by IMS.¹⁰² *Bower's* and *Russell's* groups developed early MALDI source with IMS.¹⁰³ More recently, *Clemmer's* group resolved ESI source with IMS.¹⁰⁴

1.3.1 Drift Tube Ion Mobility Spectrometry (DTIMS)

Originally, IMS used simple drift tubes as the separators. A drift tube has a static uniform electric field along the radial axis to direct ions towards the mass analyzer.¹⁰⁵ The drift cell is filled with inert gas, typically helium. A packet of ions is released by an ion gate. Under the influence of the weak electric field, injected ions traverse the drift region with a velocity

$$v_d = K \times E \quad (1.8)$$

$$v_d = \frac{L}{t_d} \quad E = \frac{V}{L}$$

where E corresponds to the electric field, and V is the voltage applied across the drift cell. K refers to mobility of ions which is specific to interactions between the ion and the gas molecule,

hence K contains terms of ion charge state, shape and gas pressure. Individual components within analyte packet can be separated because of differences in mobility. Drift time (t_d), based on the common concept, is determined by the velocity and the length of drift tube (L). On the other hand, considering the differences among laboratories, K is usually normalized to standard conditions, yielding the reduced mobility (K_0):

$$K_0 = \frac{L^2}{t_d V} \times \frac{273.2 \text{ K}}{T} \times \frac{P}{760 \text{ Torr}} \quad (1.9)$$

where P and T correspond to the pressure and temperature of buffer gas, respectively.¹⁰⁶ The collision cross section (Ω) can be related to the drift time according to Mason-Schamp equation.^{100, 106-108}

$$\Omega = \left(\frac{18\pi}{\mu k_B T}\right)^{1/2} \frac{eE}{16NL} \frac{T}{273.2 \text{ K}} \frac{760 \text{ Torr}}{P} t_d z \quad (1.10)$$

where z corresponds to the ion charge; k_B is the Boltzmann's constant; N is the number density of the buffer gas; and μ refers to the reduced mass of ion and buffer gas. From this relationship, we can conclude that for the ions with same charges, large species experience a stronger resistance than small ions because of collisions with gas molecules. Hence, the drift time (t_d) is longer for large ions (Figure 1-6). On the other hand, ions with more charges experience a larger force during the moving process. Therefore, they traverse more quickly. In consequence, in IMS, drift time is dependent on collision cross section, as well as ion charge state ($t_d \sim \Omega/z$). In comparison, MS separates ions according to m/z . IMS and MS, therefore, are complementary separation techniques.

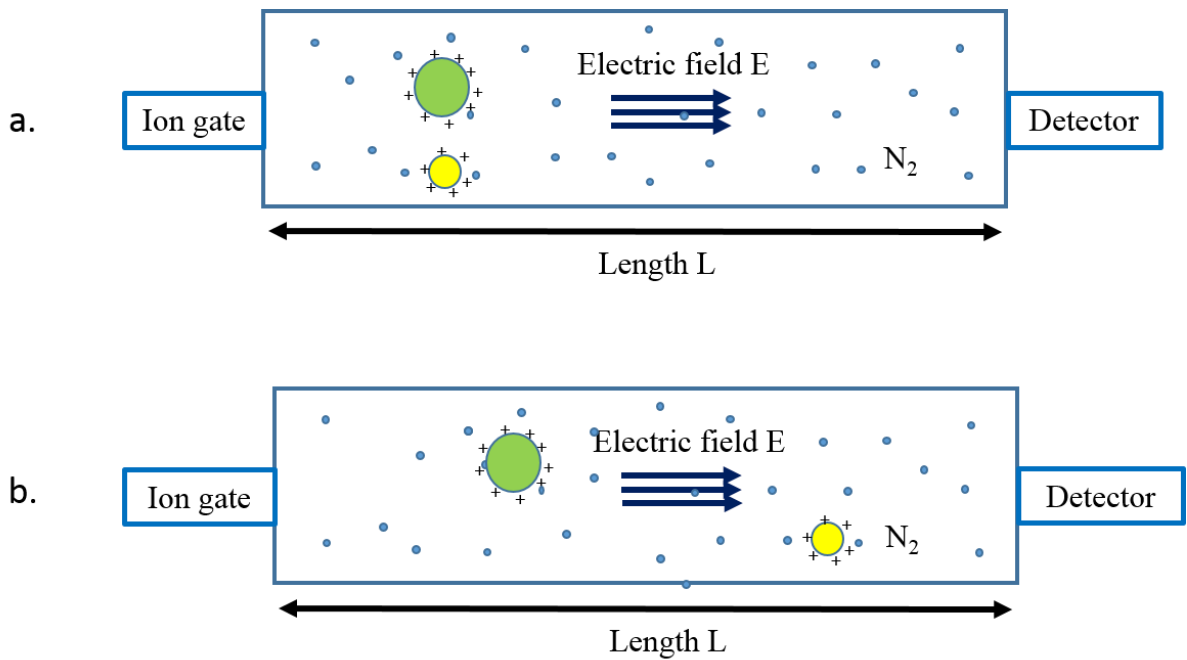


Figure 1-6 Drift Time IMS Separator (DTIMS).

A packet of ions is released by an ion gate. (a.) Under the influence of a static electric field, the ions experience collisions with buffer gas molecules. (b.) Large species experience a stronger resistance than small ions because of collisions with gas molecules. Hence, the drift time (t_d) is longer for large ions.

The CCSs determined from DTIMS provides information for ion shapes. It can be compared with data derived from X-ray crystallography and NMR spectrometry. DTIMS is superior of its high resolving power that R can reach $100 \Omega/\Delta\Omega$.¹⁰⁹ However, it suffers from poor sensitivity due to the low duty cycle and due to ion radial diffusion beyond the extreme diameter of sampling apertures.¹¹⁰ Duty cycle is related to the percentage of ions detected relative to those enter into the drift cell. This drawback can be effectively overcome by applying an ion trap before injecting ions into the drift tube, which can accumulate ions while a previous pulse is being separated.¹¹¹⁻¹¹² Another solution to improve duty cycle is to use MALDI as the ionization source, which can provide pulsed ion plume for mobility separation.¹¹³⁻¹¹⁴ Ion radial diffusion can be lowered by use of a periodic focussing DC drift tube.¹¹⁵

1.3.2 Drift Field and Resolution

The behavior of an ion drifting through buffer gas is dependent on the ratio of electric field strength to buffer gas number density, E/N .^{99, 106} At low E/N , the velocity of ions is small compared to the thermal velocity of buffer gas. In this case, the mobility is independent on the field strength and cross-section measurement report on correspond to the average of all ion orientations. Under high-field conditions, the mobility may increase or decrease, such that this regime is usually avoided.¹¹⁶⁻¹¹⁸

The IMS resolution is given by $R = t/\Delta t$. According to Revercomb and Mason¹¹⁹, it can be approximated as:

$$\frac{t}{\Delta t} \approx \left(\frac{LEze}{16k_B T \ln 2} \right)^{\frac{1}{2}} \quad (1.11)$$

where Δt corresponds to the full width at half-maximum of a peak, k_B refers to Boltzmann's constant, L is the length of the drift tube, and E is the electric field applied along the drift region. This shows that increasing the drift field or length, or decreasing the temperature is helpful to improve the resolution.

1.3.3 Collision Cross Section (CCS)

The idea of IMS is that ion packages are exposed to an electric field in the presence of a background gas. IMS separates gaseous ions according to Ω/z , where Ω and z are the collision cross section and the charge state, respectively. To a first approximation, collision cross section represents a rotationally averaged projection area involved in ion-buffer gas collisions.¹²⁰ CCS can represent protein "size". For example, unfolded proteins will have larger Ω values than tightly folded species (Figure 1-7). In order to calculate the collision cross section, *Shvartsburg* and *Jarrold* developed a program called MOBCAL to determine theoretical CCS values based on input coordinate files, derived from X-ray crystallography, NMR studies, or MD simulations.¹²¹⁻¹²³ Three models are commonly used in MOBCAL: Projection approximation (PA),¹²⁴ exact hard sphere scattering method (EHSS),¹²⁵ and trajectory method (TM).¹²² The simplest approach is the PA. The CCS is determined by averaging all possible orientations when the particle rotates. However, this method ignores the long-distance interactions and the scattering process between the ion and buffer gas. As an improvement, the EHSS method calculates CCSs by averaging the momentum transfer cross section. It takes into account scattering and collision process, but does not consider the effects of long range interactions.¹²⁶ TM is regarded as the most reliable and accurate method. It combines all the effects including

scattering events, long-range interactions and multiple collisions. The only weakness we have to consider is that this method is time consuming.

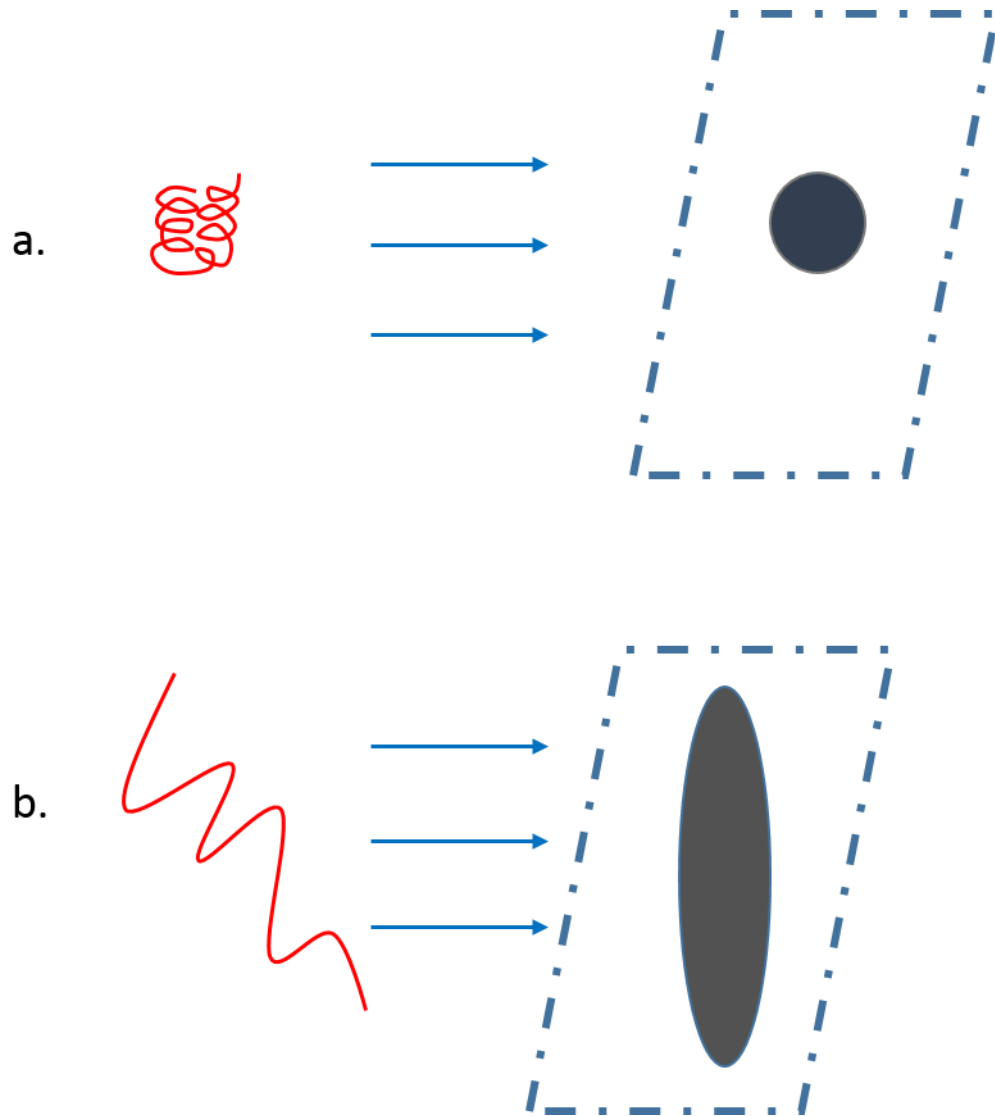


Figure 1-7 An Approximate Schematic Diagram of Collision Cross Section (CCS).

To a first approximation, collision cross section represents a rotationally averaged projection area involved in ion-buffer gas collisions. a. represents the small CCS of folded protein. b. shows that an extended protein has a larger CCS.

1.3.4 Travelling Wave Ion Mobility Spectrometry (TWIMS)

A different approach to mobility separate ions is using travelling wave voltages. This preference is caused by the availability of commercial TWIMS instrument in the recent years.¹¹⁰ A TWIMS device comprises a series of ring electrodes that form a stacked ring ion guides.¹²⁷ The ion guides are arranged orthogonally to the ion transmission direction. Opposite phases of a radio frequency (RF) voltage are applied to adjacent electrodes to provide radial potential barrier (Figure 1-8).¹²⁸ The ions are trapped in these potential wells so that ion diffusion can be minimized during transmission process. If the ion traps are sufficiently deep, some ions can be prevented and never exit from the cell.¹²⁹ In order to propel ions, a direct current (DC) voltage is superimposed on the RF voltage to a pair of ring electrodes. This DC voltage is transient on one pair of rings and then switches to next pair downstream at regular time. Therefore, the potential hills are generated continuously and provide propagating pulse that push the ions forward (travelling wave ion guide - TWIG). There is nitrogen gas filled in the drift cell to provide collisions between ions and buffer gas molecules.

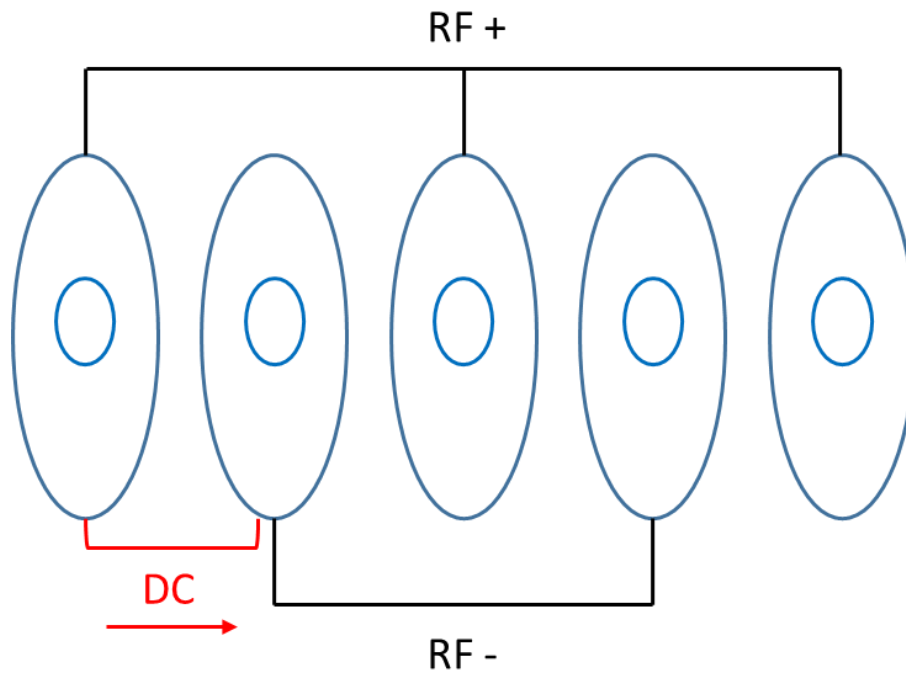


Figure 1-8 Travelling Wave Ion Guide (TWIG).

Opposite phases of a radio frequency (RF) voltage are applied to adjacent electrodes to provide ion confinement. A direct current (DC) voltage is superimposed on the RF to propel ions forward. This DC voltage is transient and it propagates to downstream at regular intervals.

Ion mobility separation is achieved by the effect of travelling wave voltage and collisions with buffer gas (Figure 1-9). During the drifting process, all the ions are propelled in the direction that the wave is travelling. Ion species of high mobility are more likely to keep up with the waves. While the ions that have low mobility are impeded by collisions and slip behind the waves. Therefore, different structural ions would exit at different time and mobility-based separation takes place. It has been found empirically¹³⁰ that t_d in TWIMS is described as

$$\Omega = z \times F \times t_d^B \quad (1.12)$$

where F and B are constant that have to be determined experimentally. Hence, TWIMS data have to be calibrated based on drift tube reference values.^{105, 107, 131-132}

For the Synapt instrument used in this work (Figure 1-5), there are three TWIGs. The trap ion guide is used to accumulate ions and then release them into the IM ion guide. The IM ion guide is the ion mobility separator. It is gas tight except the entrance and exit apertures. The transfer ion guide can transport the separated ions into the TOF mass analyzer.

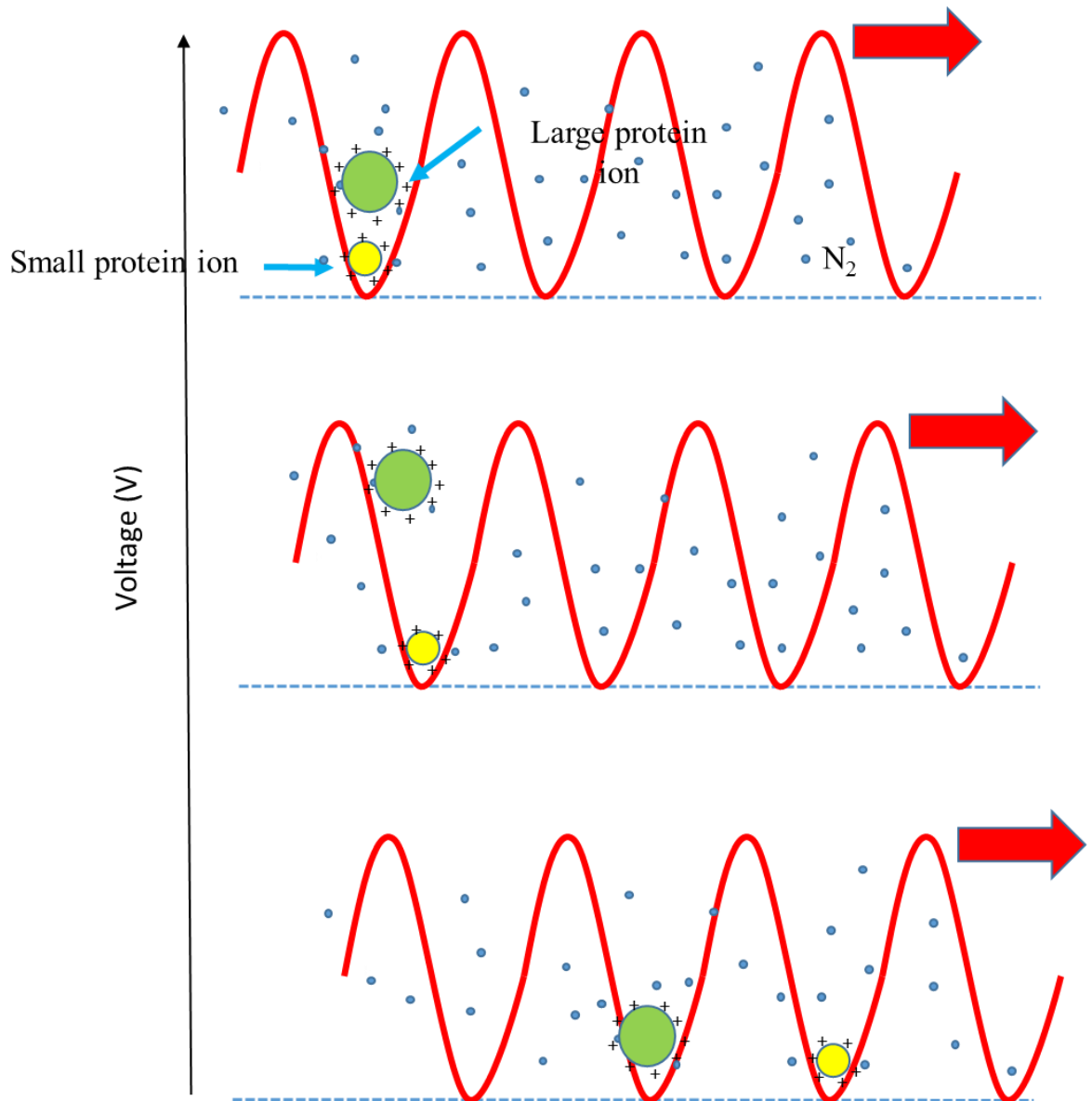


Figure 1-9 Travelling Wave IMS Separator.

A T-wave is formed under the effect of combination of RF and transient DC voltage. Ion species of high mobility are more likely to keep up with the waves. Ions that have low mobility are impeded by collisions and slip behind the waves.

The characteristics of mobility separation of TWIMS is very similar to those of DTIMS. The advantage of TWIMS includes high transmission efficiency due to the ion accumulation and radial ion confinement.¹¹⁰ The transit time of ions through the collision cell is reduced which makes it more compatible for combining with a tandem mass spectrometer where fast mass scanning or switching is required. For example, application of TWIMS increased the rate at which biological samples could be screened, which enables the efficient detection and identification of impurities in therapeutic drugs.¹³³ The sensitivity is also not compromised when acquiring mobility mode.¹²⁷ However, the resolution of TWIMS is not as high as in DTIMS. Recently, there have been improvements to increase the resolution by raising TWIMS operating pressure, using a helium entry cell, and increasing field and amplitude of the T-wave.¹³⁴ All these factors helped enhancing resolution to $45 (\Omega / \Delta\Omega)$, which is four times that of the original version.

1.4 Scope of this Thesis

In this work, we employ TWIMS combined with mass spectrometry to investigate the conformational properties of electrosprayed protein ions in the gas phase. The drift time data obtained from experiments have to be calibrated based on reference CCS values. The calibrated CCSs can be compared with the values calculated from model structures obtained by X-ray crystallography and NMR spectroscopy and molecular dynamics (MD) simulations

In chapter 2, we revisit the calibration issue related to collisional activation. Existing protocol was found to be quite convoluted and do not address a key problem, i.e, the fact that Ω value can be strongly dependent on experimental conditions. We propose a simplified calibration procedure and we try to clarify the calibration condition.

In chapter 3, the question whether electrosprayed protein ions retain solution-like conformations remains is addressed. We employ TWIMS to compare the gas-phase CCSs with the values calculated from other techniques which provide condensed phase structures. We also use MD simulations to provide computational structures as another reference. In addition, we use two types of electrospray ionization sources to perform the IMS experiments on four different proteins. Thus, comparisons between the two sources can be made in terms of “softness”.

1.5 References

1. Wu, Y.; Engen, J. R., *Analyst* **2004**, *129* (4), 290-296.
2. Pauling, L.; Corey, D. R.; Branson, H. R., *Proc. Natl. Acad. Sci. U.S.A.* **1951**, *37*, 205-210.
3. Pauling, L.; Corey, R. B., *Proc Natl Acad Sci USA* **1951**, *37* (5), 251-256.
4. Southall, N. T.; Dill, K. A.; Haymett, A. D. J., *J. Phys. Chem. B* **2002**, *106*, 521-533.
5. Widom, B.; Bhimalapuram, P.; Koga, K., *Phys. Chem. Chem. Phys.* **2003**, *5*, 3085-3093.
6. Anfinsen, C. B., *Science* **1973**, *181*, 223-230.
7. Miranker, A.; Robinson, C. V.; Radford, S. E.; Dobson, C. M., *FASEB J.* **1996**, *10*, 93-101.
8. Bai, Y.; Sosnick, T. R.; Leland, M.; Englander, S. W., *Science* **1995**, *269* (5221), 192-197.
9. Currin, A.; Swainston, N.; Day, P. J.; Kell, D. B., *Chem. Soc. Rev.* **2015**, *44* (5), 1172-1239.
10. Ingle, D. J.; Crouch, S. R., *Spectrochemical Analysis*. Prentice Hall, New Jersey, 1988.
11. Nienhaus, K.; Nienhaus, G. U., Probing Heme Protein-Ligand Interactions by UV/Visible Absorption Spectroscopy. In *Protein-Ligand Interactions*, Ulrich Nienhaus, G., Ed. Humana Press: 2005; Vol. 305, pp 215-241.

12. Engler, N.; Ostermann, A.; Gassmann, A.; Lamb, D. C.; Prusakov, V. E.; Schott, J.; Schweitzer-Stenner, R.; Parak, F. G., *Biophys. J.* **2000**, 78 (4), 2081-2092.
13. Kelly, S. M.; Price, N. C., *Curr Protein Pept Sci.* **2000**, 1 (4), 349-384.
14. Chen, Y.; Barkley, M. D., *Biochemistry* **1998**, 37, 9976-9982.
15. Rhodes, G., *Crystallography Made Crystal Clear*. 2nd ed.; Academic Press: San Diego, 2000; p pp 29-37.
16. Read, R. J., *Structure* **1996**, 4 (1), 11-14.
17. Moffat, K., *Chem.Rev.* **2001**, 101, 1569-1581.
18. Petsko, G. A.; Ringe, D., *Curr. Op. Chem. Biol.* **2000**, 4 (1), 89-94.
19. Woodward, C., *Trends Biochem. Sci.* **1993**, 18, 359-360.
20. Li, R.; Woodward, C., *Protein Sci.* **1999**, 8 (8), 1571-1590.
21. Cala, O.; Guilliere, F.; Krimm, I., *Anal. Bioanal. Chem.* **2014**, 406 (4), 943-956.
22. Unger, V. M., *Curr. Op. Struct. Biol.* **2001**, 11 (5), 548-554.
23. Urnavicius, L.; Zhang, K.; Diamant, A. G.; Motz, C.; Schlager, M. A.; Yu, M. M.; Patel, N. A.; Robinson, C. V.; Carter, A. P., *Science* **2015**, 347 (6229), 1441-1446.
24. Griffiths, I. W., *Rapid communications in mass spectrometry : RCM* **1997**, 11 (1), 3-16.
25. Munson, M. S. B.; Field, F. H., *J. Am. Chem. Soc.* **1966**, 88 (12), 2621-&.

26. Tanaka, K.; Waki, H.; Ido, Y.; Akita, S.; Yoshida, Y.; Yoshida, T.; Matsuo, T., *Rapid communications in mass spectrometry : RCM* **1988**, 2 (8), 151-153.
27. Markides, K.; Gräslund, A., *The Royal Swedish Academy of Sciences* **2002**, 1-13.
28. Chang, W. C.; Huang, L. C.; Wang, Y. S.; Peng, W. P.; Chang, H. C.; Hsu, N. Y.; Yang, W. B.; Chen, C. H., *Anal. Chim. Acta* **2007**, 582, 1-9.
29. Keller, B. O.; Li, L., *J. Am. Soc. Mass Spectrom.* **2001**, 12, 1055-1063.
30. Fenn, J. B., *Angew. Chem. Int. Ed.* **2003**, 42, 3871-3894.
31. El-Aneed, A.; Cohen, A.; Banoub, J., *Appl. Spectrosc. Rev.* **2009**, 44 (3), 210-230.
32. Taylor, G.; Mcewan, A. D., *J. Fluid Mech* **1965**, 22, 1-15.
33. Iavarone, A. T.; Williams, E. R., *J. Am. Chem. Soc.* **2003**, 125, 2319-2327.
34. Rayleigh, L., *phil. Mag.* **1882**, 14 (87), 184-186.
35. Dole, M.; Mack, L. L.; Hines, R. L.; Mobley, R. C.; Ferguson, L. D.; Alice, M. B., *J. Chem. Phys.* **1968**, 49, 2240-2249.
36. Iribarne, J. V.; Thomson, B. A., *J. Chem. Phys.* **1976**, 64, 2287-2294.
37. Nguyen, S.; Fenn, J. B., *Proc. Natl. Acad. Sci. U.S.A.* **2007**, 104, 1111-1117.
38. Zhan, D.; Rosell, J.; Fenn, J. B., *J. Am. Soc. Mass Spectrom.* **1998**, 9, 1241-1247.
39. Fenn, J. B., *J. Am. Soc. Mass Spectrom.* **1993**, 4, 524-535.
40. Gamero-Castaño, M.; de la Mora, F. J., *Anal. Chim. Acta* **2000**, 406, 67-91.
41. Kebarle, P.; Tang, L., *Anal. Chem.* **1993**, 65, 972A-986A.

42. Gamero-Castaño, M.; de la Mora, F., *J. Mass Spectrom.* **2000**, *35*, 790-803.
43. Hogan, C. J.; Carroll, J. A.; Rohrs, H. W.; Biswas, P.; Gross, M. L., *Anal. Chem.* **2009**, *81*, 369-377.
44. Labowsky, M.; Fenn, J. B.; Fernandez de la Mora, J., *Anal. Chim. Acta* **2000**, *406*, 105-118.
45. Kebarle, P.; Verkerk, U. H., *Mass Spec. Rev.* **2009**, *28* (6), 898-917.
46. Heck, A. J. R.; Van den Heuvel, R. H. H., *Mass Spectrom. Rev.* **2004**, *23*, 368-389.
47. Ahadi, E.; Konermann, L., *J. Phys. Chem. B* **2012**, *116*, 104-112.
48. Patriksson, A.; Marklund, E.; van der Spoel, D., *Biochem* **2007**, *46*, 933-945.
49. Steinberg, M. Z.; Breuker, K.; Elber, R.; Gerber, R. B., *Phys. Chem. Chem. Phys.* **2007**, *9*, 4690-4697.
50. Fersht, A. R., *Structure and Mechanism in Protein Science*. W. H. Freeman & Co.: New York, 1999.
51. Rose, G. D.; Geselowitz, A. R.; Lesser, G. J.; Lee, R. H.; Zehfus, M. H., *Science* **1985**, *229* (4716), 834-838.
52. Kuprowski, M. C.; Konermann, L., *Anal. Chem.* **2007**, *79*, 2499-2506.
53. Dobo, A.; Kaltashov, I. A., *Anal. Chem.* **2001**, *73*, 4763-4773.
54. Konermann, L.; Douglas, D. J., *J. Am. Soc. Mass Spectrom.* **1998**, *9*, 1248-1254.
55. Konermann, L.; Douglas, D. J., *Biochemistry* **1997**, *36*, 12296-12302.

56. Konermann, L.; Rodriguez, A. D.; Liu, J., *Anal. Chem.* **2012**, *84*, 6798–6804.
57. Konermann, L.; Ahadi, E.; Rodriguez, A. D.; Vahidi, S., *Anal. Chem.* **2013**, *85*, 2-9.
58. Covey, T. R.; Thomson, B. A.; Schneider, B. B., *Mass Spectrom. Rev.* **2009**, *28*, 870-897.
59. Wang, W.; Kitova, E. N.; Klassen, J. S., *Anal. Chem.* **2003**, *75*, 4945-4955.
60. Wilm, M.; Mann, M., *Anal. Chem.* **1996**, *68*, 1-8.
61. Wilm, M.; Shevchenko, A.; Houthaeve, T.; Breit, S.; Schweigerer, L.; Fotsis, T.; Mann, M., *Nature* **1996**, *379*, 466-469.
62. Benesch, J. L. P.; Ruotolo, B. T.; Simmons, D. A.; Robinson, C. V., *Chem. Rev.* **2007**, *107*, 3544-3567.
63. Yuill, E. M.; Sa, N. Y.; Ray, S. J.; Hieftje, G. M.; Baker, L. A., *Anal. Chem.* **2013**, *85* (18), 8498-8502.
64. Oosterkamp, A. J.; Gelpi, E.; Abian, J., *J. Mass Spectrom.* **1998**, *33* (10), 976-983.
65. Chang, Y. Z.; Chen, Y. R.; Her, G. R., *Anal. Chem.* **2001**, *73* (21), 5083-5087.
66. Bendahl, L.; Hansen, S. H.; Olsen, J., *Rapid Commun. Mass Spectrom.* **2002**, *16* (24), 2333-2340.
67. Jecklin, M. C.; Touboul, D.; Bovet, C.; Wortmann, A.; Zenobi, R., *J. Am. Soc. Mass Spectrom.* **2008**, *19*, 332-343.
68. Marginean, I.; Page, J. S.; Tolmachev, A. V.; Tang, K. Q.; Smith, R. D., *Anal. Chem.* **2010**, *82*, 9344-9349.

69. Grimm, R. L.; Beauchamp, J. L., *Anal. Chem.* **2002**, *74* (24), 6291-6297.
70. Geromanos, S.; Freckleton, G.; Tempst, P., *Anal. Chem.* **2000**, *72* (4), 777-790.
71. Juraschek, R.; Dulcks, T.; Karas, M., *J. Am. Soc. Mass Spectrom.* **1999**, *10*, 300-308.
72. Karas, M.; Bahr, U.; Dulcks, T., *Front Sci. Ser.* **2000**, *366* (6-7), 669-676.
73. Gabelica, V.; Vreuls, C.; Filee, P.; Duval, V.; Joris, B.; De Pauw, E., *Rapid Commun. Mass Spectrom.* **2002**, *16*, 1723-1728.
74. Bovet, C.; Wortmann, A.; Eiler, S.; Granger, F.; Ruff, M.; Gerrits, B.; Moras, D.; Zenobi, R., *Protein Sci.* **2007**, *16* (5), 938-946.
75. March, R. E., *J. Mass Spectrom.* **1997**, *32* (4), 351-369.
76. Iribarne, J. V.; Dziedzic, P. J.; Thomson, B. A., *Int. J. Mass. Spectrom.* **1983**, *50*, 331-347.
77. Smith, R. D.; Loo, J. A.; Baringa, C. J.; Edmonds, C. G.; Udseth, H. R., *J. Am. Soc. Mass Spectrom.* **1990**, *1*, 53-65.
78. Mirza, U. A.; Cohen, S. L.; Chait, B. T., *Anal. Chem.* **1993**, *65*, 1-6.
79. Cox, K. A.; Julian, R. K.; Cooks, R. G.; Kaiser, R. E., *J. Am. Soc. Mass Spectrom.* **1994**, *5*, 127-136.
80. Chernushevich, I. V.; Loboda, A. V.; Thomson, B. A., *J. Mass Spectrom.* **2001**, *36* (8), 849-865.
81. Steel, C.; Henchman, M., *J. Chem. Ed.* **1998**, *75* (8), 1049-1054.
82. Stephens, W. E., *Phys. Rev.* **1946**, *69* (11-1), 691-691.

83. Cotter, R. J., *Anal. Chem.* **1999**, 71 (13), 445A-451A.
84. Verentchikov, A. N.; Ens, W.; Standing, K. G., *Anal. Chem.* **1994**, 66 (1), 126-133.
85. Mamyrin, B. A., *Int. J. Mass Spectrom.* **2001**, 206 (3), 251-266.
86. Comisar.Mb; Marshall, A. G., *Chem. Phys. Lett.* **1974**, 25 (2), 282-283.
87. Marshall, A. G., *Int. J. Mass Spectrom.* **2000**, 200 (1-3), 331-356.
88. Makarov, A., *Anal. Chem.* **2000**, 72, 1156-1162.
89. Hardman, M.; Makarov, A., *Anal. Chem.* **2003**, 75, 1699-1705.
90. Hu, Q.; Noll, R. J.; Li, H.; Makarov, A.; Hardman, M.; Cooks, R. G., *J. Mass Spectrom.* **2005**, 40, 430-443.
91. Goswami, D.; Tuske, S.; Pascal, B. D.; Bauman, J. D.; Patel, D.; Arnold, E.; Griffin, P. R., *Anal. Chem.* **2015**, 87 (7), 4015-4022.
92. Keppel, T. R.; Weis, D. D., *J. Am. Soc. Mass Spectrom.* **2015**, 26 (4), 547-554.
93. Zhang, Z. Q.; Smith, D. L., *Protein Sci.* **1993**, 2 (4), 522-531.
94. Khakinejad, M.; Kondalaji, S. G.; Maleki, H.; Arndt, J. R.; Donohoe, G. C.; Valentine, S. J., *J. Am. Soc. Mass Spectrom.* **2014**, 25 (12), 2103-2115.
95. Cornell, W. D.; Cieplak, P.; Bayly, C. I.; Gould, I. R.; Merz, K. M.; Ferguson, D. M.; Spellmeyer, D. C.; Fox, T.; Caldwell, J. W.; Kollman, P. A., *J. Am. Chem. Soc.* **1995**, 117 (19), 5179-5197.
96. Steinberg, M. Z.; Elber, R.; McLafferty, F. W.; Gerber, R. B.; Breuker, K., *ChemBioChem* **2008**, 9, 2417-2423.

97. Saikusa, K.; Fuchigami, S.; Takahashi, K.; Asano, Y.; Nagadoi, A.; Tachiwana, H.; Kurumizaka, H.; Ikeguchi, M.; Nishimura, Y.; Akashi, S., *Anal. Chem.* **2013**, 85 (8), 4165-4171.
98. Wytttenbach, T.; von Helden, G.; Bowers, M. T., *J. Am. Chem. Soc.* **1996**, 118, 8355-8364.
99. Clemmer, D. E.; Jarrold, M. F., *J. Mass Spectrom.* **1997**, 32, 577-592.
100. Konijnenberg, A.; Butterer, A.; Sobott, F., *BBA-Proteins Proteomics* **2013**, 1834 (6), 1239-1256.
101. Lee, J. W.; Kim, H. I., *Analyst* **2015**, 140 (2), 661-669.
102. Clemmer, D. E.; Hudgins, R. R.; Jarrold, M. F., *J. Am. Chem. Soc.* **1995**, 117, 10141-10142.
103. Gillig, K. J.; Ruotolo, B.; Stone, E. G.; Russell, D. H.; Fuhrer, K.; Gonin, M.; Schultz, A. J., *Anal. Chem.* **2000**, 72 (17), 3965-3971.
104. Myung, S.; Wiseman, J. M.; Valentine, S. J.; Takats, Z.; Cooks, R. G.; Clemmer, D. E., *J. Phys. Chem. B* **2006**, 110 (10), 5045-5051.
105. Bush, M. F.; Hall, Z.; Giles, K.; Hoyes, J.; Robinson, C. V.; Ruotolo, B. T., *Anal. Chem.* **2010**, 82, 9667-9565.
106. Mason, E. A.; McDaniel, E. W., *Wiley* **1988**.
107. Ruotolo, B. T.; Benesch, J. L. P.; Sandercock, A. M.; Hyung, S.-J.; Robinson, C. V., *Nat. Protocols* **2008**, 3, 1139-1152.
108. Kanu, A. B.; Dwivedi, P.; Tam, M.; Matz, L. M.; Hill, H. H., *J. Mass Spectrom.* **2008**, 43, 1-22.

109. Lanucara, F.; Holman, S. W.; Gray, C. J.; Eyers, C. E., *Nature Chemistry* **2014**, 6 (4), 281-294.
110. Pringle, S. D.; Giles, K.; Wildgoose, J. L.; Williams, J. P.; Slade, S. E.; Thalassinos, K.; Bateman, R. H.; Bowers, M. T.; Scrivens, J. H., *Int. J. Mass Spectrom.* **2007**, 261, 1-12.
111. Hoaglund, C. S.; Valentine, S. J.; Clemmer, D. E., *Anal. Chem.* **1997**, 69 (20), 4156-4161.
112. Wytttenbach, T.; Kemper, P. R.; Bowers, M. T., *Int. J. Mass Spectrom.* **2001**, 212 (1-3), 13-23.
113. Gillig, K. J.; Ruotolo, B. T.; Stone, E. G.; Russell, D. H., *Int. J. Mass Spectrom.* **2004**, 239 (1), 43-49.
114. Woods, A. S.; Ugarov, M.; Egan, T.; Koomen, J.; Gillig, K. J.; Fuhrer, K.; Gonin, M.; Schultz, J. A., *Anal. Chem.* **2004**, 76 (8), 2187-2195.
115. McLean, J. A.; Ruotolo, B. T.; Gillig, K. J.; Russell, D. H., *Int. J. Mass Spectrom.* **2005**, 240 (3), 301-315.
116. Buryakov, I. A.; Krylov, E. V.; Nazarov, E. G.; Rasulev, U. K., *Int. J. Mass Spectrom. Ion Proc.* **1993**, 128 (3), 143-148.
117. Purves, R. W.; Guevremont, R.; Day, S.; Pipich, C. W.; Matyjaszczyk, M. S., *Rev. Sci. Inst.* **1998**, 69 (12), 4094-4105.
118. Shvartsburg, A. A.; Mashkevich, S. V.; Smith, R. D., *J. Phys. Chem. A* **2006**, 110 (8), 2663-2673.
119. Revercomb, H. E.; Mason, E. A., *Anal. Chem.* **1975**, 47 (7), 970-983.
120. Wytttenbach, T.; Bleiholder, C.; Bowers, M. T., *Anal. Chem.* **2013**, 85 (4), 2191-2199.

121. Shvartsburg, A. A.; Jarrold, M. F., *Chem. Phys. Lett.* **1996**, *261* (1–2), 86-91.
122. Shvartsburg, A. A.; Schatz, G. C.; Jarrold, M. F., *J. Chem. Phys.* **1998**, *108* (6), 2416-2423.
123. Mesleh, M. F.; Hunter, J. M.; Shvartsburg, A. A.; Schatz, G. C.; Jarrold, M. F., *J. Phys. Chem.* **1996**, *100* (40), 16082-16086.
124. Wytttenbach, T.; vonHelden, G.; Batka, J. J.; Carlat, D.; Bowers, M. T., *J. Am. Soc. Mass Spectrom.* **1997**, *8* (3), 275-282.
125. Shvartsburg, A. A.; Smith, R. D., *J. Am. Soc. Mass Spectrom.* **2008**, *19* (9), 1286-1295.
126. Zubarev, R. A.; Horn, D. M.; Fridriksson, E. K.; Kelleher, N. L.; Kruger, N. A.; Lewis, M. A.; Carpenter, B. K.; McLafferty, F. W., *Anal. Chem.* **2000**, *72* (3), 563-573.
127. Giles, K.; Pringle, S. D.; Worthington, K. R.; Little, D.; Wildgoose, J. L.; Bateman, R. H., *Rapid communications in mass spectrometry : RCM* **2004**, *18* (20), 2401-14.
128. Tolmachev, A. V.; Kim, T.; Udseth, H. R.; Smith, R. D.; Bailey, T. H.; Futrell, J. H., *Int. J. Mass Spectrom.* **2000**, *203* (1-3), 31-47.
129. Lynn, E. C.; Chung, M. C.; Han, C. C., *Rapid communications in mass spectrometry : RCM* **2000**, *14* (22), 2129-2134.
130. Wildgoose, J.; Giles, K.; Pringle, S. D.; Koeniger, S. L.; Valentine, J. S.; Bateman, R. H.; Clemmer, D. E., A comparison of travelling wave and drift tube ion mobility separations. In *Proc. 54th ASMS Conference on Mass Spectrometry & Allied Topics*, Seattle, WA.
131. Shvartsburg, A. A.; Smith, R. D., *Anal. Chem.* **2008**, *80*, 9689–9699.
132. Lietz, C. B.; Yu, Q.; Li, L. J., *J. Am. Soc. Mass Spectrom.* **2014**, *25* (12), 2009-2019.

133. Esquenazi, E.; Daly, M.; Bahrainwala, T.; Gerwick, W. H.; Dorrestein, P. C., *Bioorg. Med. Chem.* **2011**, *19* (22), 6639-6644.
134. Giles, K.; Williams, J. P.; Campuzano, I., *Rapid Commun. Mass Spectrom.* **2011**, *25*, 1559-1566.

Chapter 2 - Calibration Issues in TWIMS

2.1 Introduction

IMS separates gaseous ions according to Ω/z , where Ω and z are the collision cross section and the charge state, respectively. To a first approximation, Ω represents a rotationally averaged projection area.¹ Ion packages are exposed to an electric field in the presence of a background gas. In drift tube IMS the electric field E is static, and the ions traverse a drift region of length L . Ω can then be determined using the relationships²⁻⁴

$$\Omega = z \times C \times t_d \quad (2.1a)$$

$$C = \frac{eE}{16NL} \left(\frac{18\pi}{\mu k_B T} \right)^{1/2} \frac{760 \text{ Torr}}{p} \frac{T}{273.2 \text{ K}} \quad (2.1b)$$

with the reduced mass μ , elementary charge e , gas number density N , temperature T , Boltzmann's constant k_B , and gas pressure p .

Recent years have witnessed the rapid growth of traveling wave (TW) IMS, where ions “surf” on DC waves within a stacked-ring RF ion guide.⁴⁻⁷ The primary difference from DTIMS is that the electric field is not constant and uniform. The transit time decreases with mobility due to the pulsed voltage. It has been found empirically⁸ that t_d in TWIMS is related to Ω via

$$\Omega = z \times F \times t_d^B \quad (2.2)$$

where F and B cannot be calculated from first principles. (eq. 2.1) Instead, TWIMS data have to be calibrated using drift tube reference values Ω_{ref} obtained on the basis of eq. 2.1.^{3, 6, 9-13}

Extracting quantitative structural information from IMS data is surprisingly difficult. An experimental Ω value represents a single number that may be consistent with many different analyte conformations. Several methods have been developed for predicting Ω values of model structures, but these methods yield results that can differ by 30% or more.^{1, 14} X-ray data are often assumed to provide plausible gas phase model structures, although crystal packing and residual water provide an environment that is very different from the vacuum.¹⁵ Molecular dynamics (MD) simulations provide insights into the behavior of proteins in the absence of solvent,¹⁶⁻¹⁹ but MD force fields are parametrized for bulk solution.²⁰ Eq. 2.1, which provides the foundation of macromolecular IMS, only represents an approximate solution of a rigorous kinetic treatment.²¹ The commonly used approach of calibrating TWIMS Ω values measured in N₂ on the basis of published He drift tube data may introduce additional issues.^{7-8, 18, 22-26} Briefly, the mobility in He is higher than that in N₂²⁷, at a given pressure, lower T-wave amplitude has to be used in with He. This can be explained that the separation has a high mobility limit, so that ion species above this limit would just surf on a single wave without mobility separation. Only the ions below the limit can be overtaken by the wave and experience the forward and reverse fields of the pulse.²⁸ However, the lower amplitudes has been proved empirically as a result of lower gas pressure⁴⁻⁵, which causes lower resolution. On the other hand, in order to achieve a high resolution, increasing N₂ pressure can give rise to another problem that a higher gas flow rate is applied and more energy is required to drive ions, which results in ion losses through scattering and fragmentation.²⁹

Like other TWIMS calibration strategies,³⁰⁻³² the procedure used here relies on reference data Ω_{ref} measured in He. Calibrated TWIMS Ω values therefore represent “effective” He collision cross-sections, although TWIMS uses N₂ as IMS gas.^{10, 33} This is justified because calibration

should correct for systematic differences between mobility in He and in N₂. F in eq. 2.2 is occasionally expressed as $F = C \times A$, where A is an empirical constant and C is defined in eq. 2.1b.^{9,34} This notation suggests that F follows a $\mu^{-1/2}$ dependence with $\mu = mM/(m+M)$, where m and M are the gas and analyte masses, respectively. To our knowledge, it has never been proven that A is independent of μ .⁸ Therefore, the assumption that F is proportional to $\mu^{-1/2}$ seems unjustified. Existing TWIMS calibration protocols nonetheless advocate a $\mu^{-1/2}$ correction.^{3,10} Luckily, this correction is negligible for proteins, where $M \gg m$ such that $\mu \approx m$. For example, Hb has $\mu = 27.99$ Da, whereas Ubq has $\mu = 27.91$ Da resulting in $\Delta(\mu^{-1/2}) \approx 0.1\%$. Similar considerations apply to measured t_d values which, strictly speaking, should be corrected for the time that the ions spend outside the drift region. This issue is important for some instruments,¹⁰ but it is insignificant for the TWIMS device considered here. The TWIMS t_d correction is on the order of 0.5% and its weak $(m/z)^{1/2}$ dependence implies that different analytes are affected to a very similar extent.³ In summary, μ and t_d corrections are unnecessary for the type of instrument used here, considering (i) the empirical origin eq. 2.2⁸ and (ii) the small magnitude of these corrections which is within the scatter of the calibration plots.

2.2 Experimental

2.2.1 Sample Preparation

Bovine ubiquitin (Ubq, 8565 Da), horse heart cytochrome c (Cyt, 12359 Da), and equine holo-myoglobin (hMb, 17568 Da) were purchased from Sigma (St. Louis, MO). The calibrant mix consisted of 10 μ M Ubq, Cyt, and hMb in 49:49:2 (v/v/v) methanol/water/acetic acid (pH 2.2).

Heme loss from hMb under these non-native solution conditions generates apo-myoglobin (aMb, 16952 Da).

2.2.2 Instrument Settings

Measurements were conducted on a Synapt HDMS time-of-flight mass spectrometer (Waters, Milford, MA).⁴⁻⁵ Regular ESI-MS experiments employed the standard Z-spray source at a capillary voltage of 2.8 kV and a desolvation gas flow rate of 500 L h⁻¹. Solutions were infused at 5 μ L min⁻¹. The source (backing) pressure was adjusted to 5 mbar by a SpeediValve on the scroll pump. The extraction cone was set to 1 V, the cone gas flow rate was 50 L h⁻¹, while the source and desolvation temperatures were 25°C and 40 °C, respectively. The IMS settings refer to the ion trap, ion mobility cell and transfer cell. The trap collision energy was 2 V, the trap wave velocity was 100 m s⁻¹ and trap wave height was 0.1 V. Trap bias was 9 V for maintaining strong signals of the denatured protein complex. The IMS wave height was set to 6.5 V at 300 m s⁻¹. The transfer collision energy was 4 V at 247 m s⁻¹, and the transfer wave height was 4 V. Other instrument parameters were as follows: trap entrance 1 V, IMS entrance 6.7 V, IMS exit 0 V, transfer entrance 1 V, and transfer exit 1 V. The trap release time was 500 μ s. TWIG pressures were 1.58×10^{-2} mbar in the trap (corresponding to trap gas “off”), while 0.5 mbar N₂ served as IMS gas. It will be seen that these instrument settings provide very gentle conditions with a minimum of ion activation when used in combination with a low sample cone voltage (5 V). For collisional heating experiments the sample cone voltage was raised up to 120 V.

2.2.3 TWIMS Calibration

Calibration was performed by measuring TWIMS profiles of the Ubq/Cyt/aMb calibrant mix for each set of experiments. Ion activation settings and calibrant peak selection are discussed below. Linear regression was performed by employing eq. 2.2 in the form

$$\ln(\Omega_{ref}/z) = R + B\ln(t_d) \quad (2.3)$$

to determine the slope B and intercept $R = \ln(F)$. Drift tube reference data Ω_{ref} are summarized in Table 1.³⁰⁻³² Ω values were then determined from measured t_d values according to

$$\Omega = z \times \exp[R + B\ln(t_d)] \quad (2.4)$$

Table 1.

Literature collision cross sections Ω_{ref} of three calibrant proteins measured on drift tube instruments with He buffer gas, using high ion injection energies to promote protein unfolding in the gas phase. The proteins were electrosprayed from denaturing solutions. For matching these species in TWIMS it is necessary to employ collisional heating (e.g., sample cone = 100 V), and to pick the most unfolded species (with the largest t_d) from the corresponding TWIMS profiles.

z	Ubq (bovine) ³⁰	Cyt (horse) ³¹	aMb (horse) ³²
6	1525	-	-
7	1580	-	-
8	1622	2061	-
9	1649	2215	-
10	1732	2226	2796
11	1802	2303	2949
12	-	2335	3048
13	-	2391	3140
14	-	2473	3147
15	-	2579	3233
16	-	2679	3319
17	-	2723	3391
18	-	2766	3490
19	-	-	3577
20	-	-	3689
21	-	-	3736
22	-	-	3821

2.3 Results and Discussion

TWIMS data cannot be converted to Ω values using first principles. Instead, it is necessary to calibrate TWIMS t_d values on the basis of published drift tube Ω_{ref} data.^{3, 6, 9-13} Currently, there are few potential calibrant ions with reported CCS values excess 3500 Å².³ A calibrant mix comprising Ubq, Cyt, and aMb in denaturing solution is commonly used for this purpose.^{3, 9} The relationship between T-wave drift time and CCS is defined by these smaller ions and then is extrapolated to larger value. “Ideal” calibrants exhibit properties that are condition-independent, e.g., mass calibration can be performed using salt clusters with m/z values that remain unchanged for any possible instrument settings. For Ω calibration it would be ideal to use reference analytes that exhibit a similar level of robustness. With this in mind, we examined the behavior of the Ubq/Cyt/aMb calibrant mix. The proteins were exposed to different levels of collisional activation by altering the sample cone voltage. The t_d values of low charge state calibrant ions increase dramatically as the cone voltage is raised (exemplified in Figure 2-1 for Ubq 6+, Cyt 8+, and aMb 12+). Similar cone-dependent changes were observed for Ubq 7+ and 8+, Cyt 9+ to 12+, and aMb 10+ to 16+. In contrast, ions in higher charge states exhibit profiles that are independent of cone voltage (Figure 2-1, Ubq 11+, Cyt 18+, aMb 22+). Cone voltages greater than 100 V start to cause calibrant breakdown by CID (Figure 2-2),³⁵ thereby identifying the upper limit of the useful parameter space.

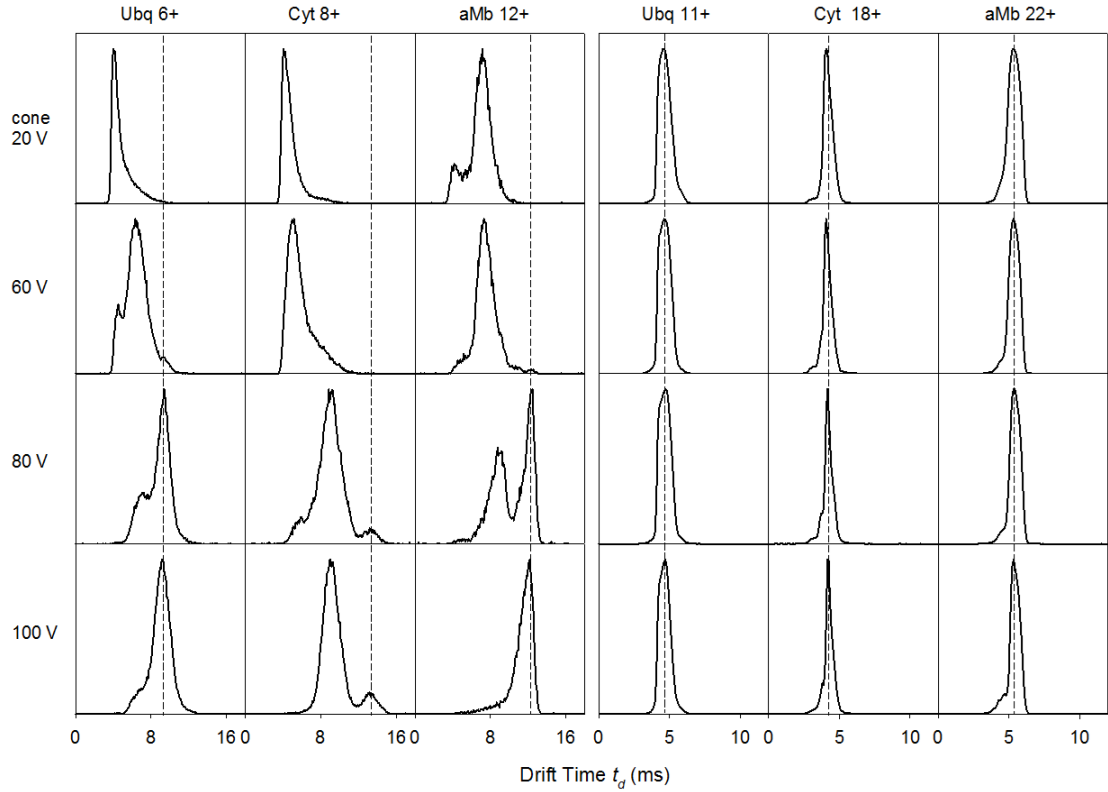


Figure 2-1 Effects of sample cone voltage on the TWIMS profiles of the Ubq/Cyt/aMb calibrant mix.

The four rows represent data for cone voltages of 20 V, 60 V, 80 V, and 100 V. Each column depicts data for a certain protein ion, as noted along the top. Vertical dashed lines indicate the peak positions observed for the most unfolded species at a cone voltage of 100 V.

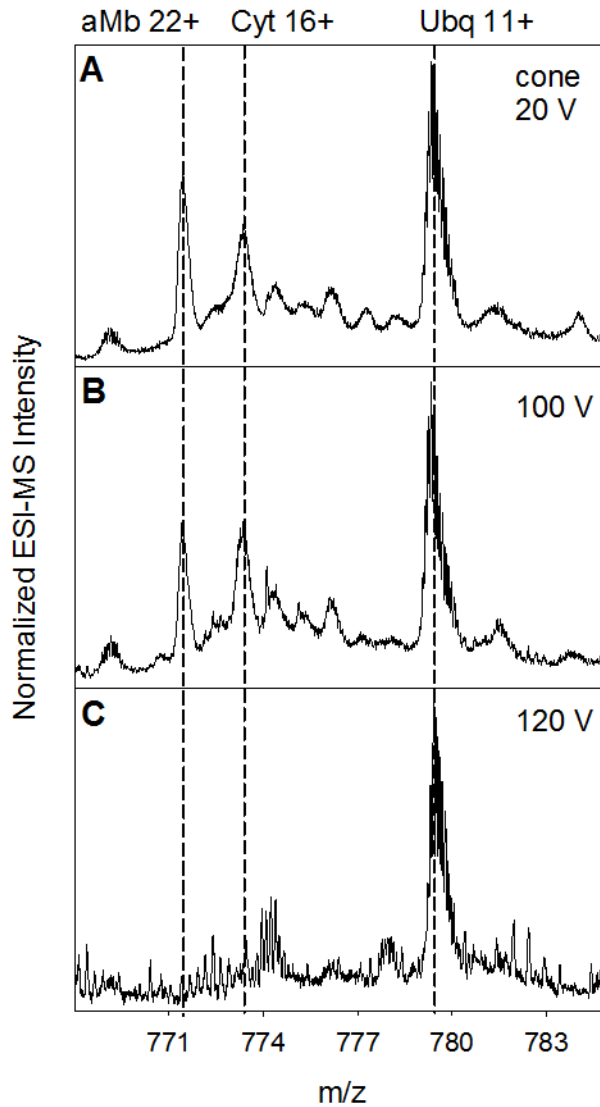


Figure 2-2 Partial ESI mass spectra, showing the appearance of CID.

High charge state range of the Ubq/Cyt/aMb calibration mix at a sample cone voltage of 20 V (A), 100 V (B), and 120 V (C) . Note the degradation of the aMb and Cyt signals in panel C due to CID.

The fact that the TWIMS profiles of many calibrant ions depend on the level of collisional activation introduces problems.^{12, 33} A reliable calibration requires TWIMS and drift tube reference data to be acquired using the same level of activation. One strategy to approach this regime is the use of TWIMS conditions that are as gentle as possible to promote the presence of compact calibrant conformers. One then has to hope that these TWIMS conditions produce structures equivalent to those observed in gentle drift tube IMS experiments. Unfortunately, given the vastly different instrument architecture of TWIMS and drift tube IMS, it cannot be guaranteed that calibrant ions experience comparable conditions. Thus, there is a danger of introducing systematic errors, as it is unclear whether calibrant ions in TWIMS and drift tube IMS share the same structures. Also, gentle conditions tend to produce weak signals due to low ion transmission.¹⁰

Here we propose a modified TWIMS calibration strategy. Instead of using gentle conditions we expose the Ubq/Cyt/aMb calibrant mix to a maximum level of ion activation (sample cone 100 V). We then pick the most unfolded component in the TWIMS profile of each calibrant ion, e.g., for Cyt 8+ we select the feature at 13.2 ms (dashed line, bottom row of Figure 2) instead of focusing on the signal at $t_d \approx 9$ ms. These TWIMS data are then matched to published drift tube Ω_{ref} values³⁰⁻³² that were obtained with high injection energies (Supporting Table 1). This strategy does not rely on the assumption that TWIMS and drift tube measurements share the same level of softness. Instead, the use of extensively unfolded conformers just below the CID threshold provides a less ambiguous basis for TWIMS calibration. Figure 2-3A illustrates that a calibration plot obtained under such harsh conditions (eq. 2.3) exhibits good linearity and covers a wide window of t_d values. TWIMS ion separation is independent of the source parameters.⁴⁻⁵ Hence, after calibration has been performed using harsh conditions one can

perform actual experiments with gentle settings that minimize ion activation. The same calibration line (Figure 2-3A) will apply, as long as the settings of the TWIMS cell and the downstream ion optics remain unchanged.³

We also generated a calibration profile under gentle conditions (sample cone 5 V), following the traditional approach where calibration and actual experiments are conducted using identical settings.^{3, 10} This procedure yields widely scattered calibration data, indicating that many of the conformers do not match those of the reference data set (Supporting Table 1). One can nonetheless generate a calibration by focusing on highly charged ions that show a linear trend (Figure 2-3B). The regression results obtained in this way are close to those of Figure 2-3A (see caption for details). This agreement reflects the fact that highly charged ions are unfolded regardless of source conditions because of their intrinsic Coulomb repulsion.^{30-32, 36} What advantages, then, are associated with the use of harsh calibration conditions? The linear region in Figure 2-3B only covers a narrow window. Using such calibration data for analytes with large t_d would require a long extrapolation (dotted line in Figure 2-3B). In contrast, the “harsh” profile remains linear over a much wider t_d range, such that Ω values can be assigned with greater confidence (Figure 2-3A). Under gentle conditions the multimodal TWIMS profiles of low charge state calibrants introduce ambiguities, as users may be uncertain which signal to select for calibration. These ions are thus usually discarded.^{3, 10, 33} These ambiguities are eliminated when calibrating under harsh conditions. Validation of the proposed strategy comes from the excellent agreement of measured Ω data with literature values (see below, Figure 3-3).

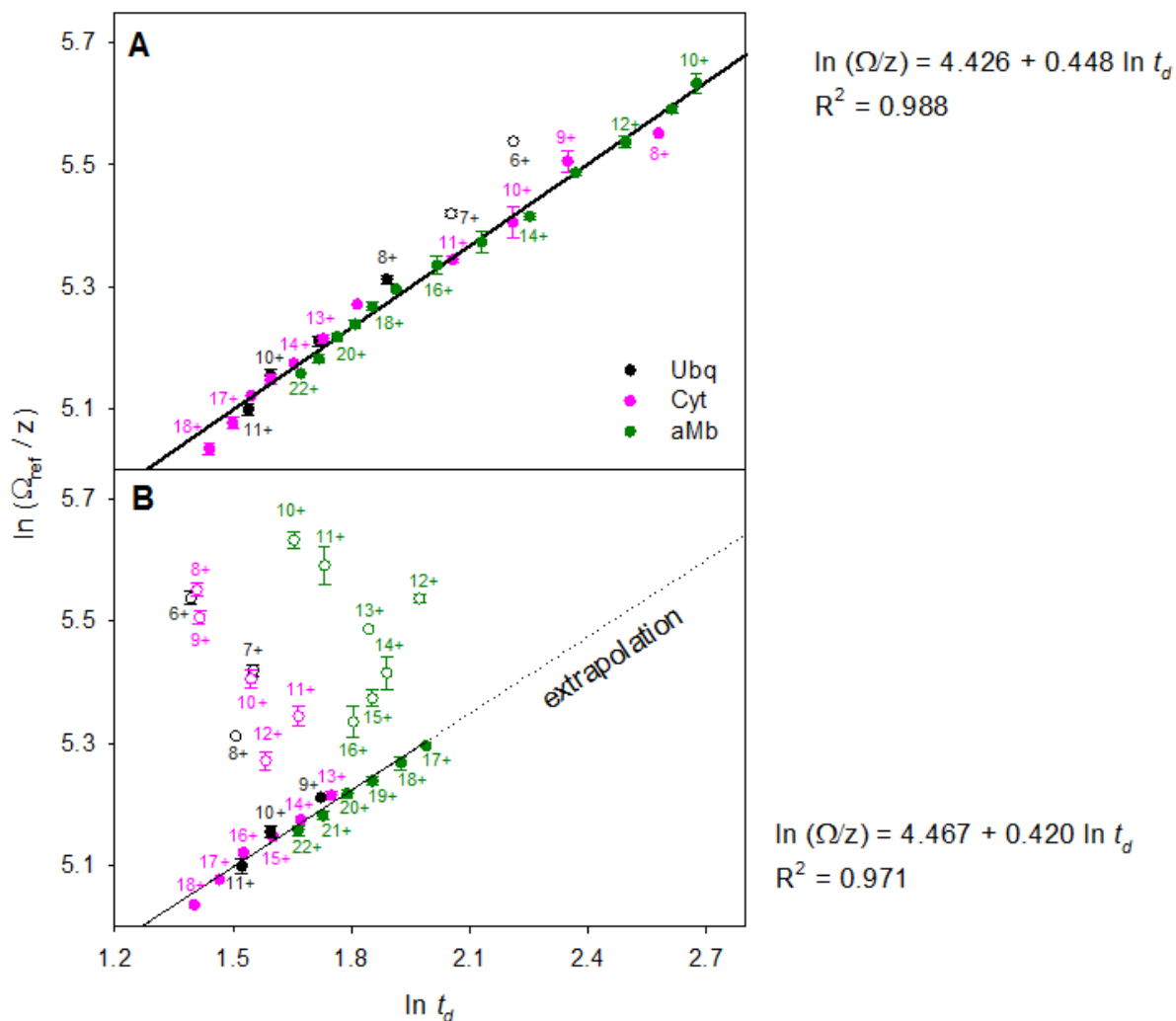


Figure 2-3 Calibration plots for the Ubq/Cyt/aMb calibrant mix.

Open symbols were not included for regression analyses. (A) Data acquired under harsh conditions (sample cone = 100 V). Each point represents the peak maximum of the most unfolded species (with the largest t_d value) in the drift time distributions. The regression line for $t_d \rightarrow \Omega$ conversion is given by $\ln(\Omega/z) = 4.426 + 0.448 \ln(t_d)$, $R^2 = 0.988$. (B) Data acquired under gentle conditions (sample cone = 5 V). Points represent peak maxima of the most intense signals in the drift time distributions. Regression line parameters: $\ln(\Omega/z) = 4.467 + 0.420 \ln(t_d)$, $R^2 = 0.971$. Error bars represent standard deviations of triplicate measurements.

The calibrant mix used here and elsewhere^{3, 10} contains horse aMb. It is worth noting that the literature Ω_{ref} values commonly used for this mix are for sperm whale aMb (<http://www.indiana.edu/~clemmer>).³ The sequences of the two variants differ in 19 positions.³⁷ Drift tube Ω_{ref} values compiled in Supporting Table 1 are for horse aMb.³² Luckily, the horse³² and sperm whale³ values are virtually identical. It is nonetheless surprising that this minor inconsistency has apparently gone unnoticed in the earlier TWIMS literature.

2.4 Conclusion

An issue unique to TWIMS is the need to calibrate measured t_d profiles using drift tube Ω_{ref} values. Here we demonstrate that the use of collisionally activated ions simplifies the calibration procedure. We employ a calibrant mixture of three denatured monomeric proteins to define the nonlinear relationship between t_d in TWIMS and Ω and then extrapolate to larger values. We simplify the algorithmic method by ignoring the negligible effect on reduced mass and the time that ions spend from transfer ion guide to mass analyzer. Since we calibrate t_d based on known Ω_{ref} measured by conventional ion mobility experiments, we hope that these TWIMS conditions are comparable to those in DTIMS. We demonstrate that the harsh condition which refers to the high activation voltages provides the most gratifying calibration curve and it results in the most closed structure to that with DTIMS. Note that the harsh condition has to be adjusted to avoid breakdown by CID. Our approach may not be optimal for very small analytes¹³ and for very large systems.¹⁰ Yet, for studies on monomeric proteins and medium-sized complexes the use of collisionally heated ions eliminates ambiguities that may be encountered otherwise.

2.5 References

1. Wyttenbach, T.; Bleiholder, C.; Bowers, M. T., *Anal. Chem.* **2013**, 85 (4), 2191-2199.
2. Konijnenberg, A.; Butterer, A.; Sobott, F., *Biochim. Biophys. Acta* **2013**, 1834 (6), 1239-1256.
3. Ruotolo, B. T.; Benesch, J. L. P.; Sandercock, A. M.; Hyung, S.-J.; Robinson, C. V., *Nat. Protocols* **2008**, 3, 1139-1152.
4. Pringle, S. D.; Giles, K.; Wildgoose, J. L.; Williams, J. P.; Slade, S. E.; Thalassinou, K.; Bateman, R. H.; Bowers, M. T.; Scrivens, J. H., *Int. J. Mass Spectrom.* **2007**, 261, 1-12.
5. Giles, K.; Pringle, S. D.; Worthington, K. R.; Little, D.; Wildgoose, J. L.; Bateman, R. H., *Rapid communications in mass spectrometry : RCM* **2004**, 18 (20), 2401-14.
6. Shvartsburg, A. A.; Smith, R. D., *Anal. Chem.* **2008**, 80, 9689-9699.
7. Scarff, C. A.; Thalassinou, K.; Hilton, G. R.; Scrivens, J. H., *Rapid communications in mass spectrometry : RCM* **2008**, 22 (20), 3297-304.
8. Wildgoose, J. L.; Giles, K.; Pringle, S. D.; Koeniger, S.; Valentine, S. J.; Bateman, R. H.; Clemmer, D. E. In *A comparison of travelling wave and drift tube ion mobility separations*, Proc. 54th ASMS Conference on Mass Spectrometry & Allied Topics, Seattle, WA, May 28-June 1st, ASMS: Seattle, WA, May 28-June 1st, 2006.
9. Smith, D. P.; Knapman, T. W.; Campuzano, I.; Malham, R. W.; Berryman, J. T.; Radford, S. E.; Ashcroft, A. E., *European journal of mass spectrometry* **2009**, 15 (2), 113-30.
10. Bush, M. F.; Hall, Z.; Giles, K.; Hoyes, J.; Robinson, C. V.; Ruotolo, B. T., *Anal. Chem.* **2010**, 82, 9667-9565.

11. Morsa, D.; Gabelica, V.; De Pauw, E., *J. Am. Soc. Mass Spectrom.* **2014**, 25 (8), 1384-1393.
12. Lietz, C. B.; Yu, Q.; Li, L., *J. Am. Soc. Mass Spectrom.* **2014**, 25, 1-11.
13. Williams, J. P.; Scrivens, J. H., *Rapid Commun. Mass Spectrom.* **2008**, 22 (2), 187-196.
14. Hogan, C. J.; Ruotolo, B. T.; Robinson, C. V.; de la Mora, J. F., *J. Phys. Chem. B* **2011**, 115 (13), 3614-3621.
15. Alexopoulos, J. A.; Guarnéa, A.; Ortega, J., *J. Struct. Biol.* **2012**, 179, 202-210.
16. Mao, Y.; Woenckhaus, J.; Kolafa, J.; Ratner, M. A.; Jarrold, M. F., *J. Am. Chem. Soc.* **1999**, 121 (12), 2712-2721.
17. Hall, Z.; Politis, A.; Bush, M. F.; Smith, L. J.; Robinson, C. V., *J. Am. Chem. Soc.* **2012**, 134, 3429-3438.
18. Fernandez-Lima, F. A.; Wei, H.; Gao, Y. Q.; Russell, D. H., *J. Phys. Chem. A* **2009**, 113 (29), 8221-8234.
19. Khakinejad, M.; Kondalaji, S. G.; Maleki, H.; Arndt, J. R.; Donohoe, G. C.; Valentine, S. J., *J. Am. Soc. Mass Spectrom.* **2014**, 25 (12), 2103-2115.
20. Hess, B.; Kutzner, C.; van der Spoel, D.; Lindahl, E., *J. Chem. Theory Comput.* **2008**, 4, 435-447.
21. Revercomb, H. E.; Mason, E. A., *Anal. Chem.* **1975**, 47 (7), 970-983.
22. Marginean, I.; Page, J. S.; Tolmachev, A. V.; Tang, K. Q.; Smith, R. D., *Anal. Chem.* **2010**, 82, 9344-9349.
23. Hilton, G. R.; Benesch, J. L. P., *J. R. Soc. Interface* **2012**, 9, 801-816.

24. Jecklin, M. C.; Touboul, D.; Bovet, C.; Wortmann, A.; Zenobi, R., *J. Am. Soc. Mass Spectrom.* **2008**, *19*, 332-343.
25. Loo, J. A., *Int. J. Mass Spectrom.* **2000**, *200*, 175-186.
26. Liu, J.; Konermann, L., *J. Am. Soc. Mass Spectrom.* **2011**, *22*, 408-417.
27. Asbury, G. R.; Hill, H. H., *Anal. Chem.* **2000**, *72* (3), 580-584.
28. Giles, K.; Wildgoose, J. L.; Langridge, D. J.; Campuzano, I., *Intl. J. Mass. Spectrom.* **2010**, *298*, 10-16.
29. Giles, K.; Williams, J. P.; Campuzano, I., *Rapid Commun. Mass Spectrom.* **2011**, *25*, 1559-1566.
30. Valentine, S. J.; Counterman, A. E.; Clemmer, D. E., *J. Am. Soc. Mass Spectrom.* **1997**, *8* (9), 954-961.
31. Shelimov, K. B.; Clemmer, D. E.; Hudgins, R. R.; Jarrold, M. F., *J. Am. Chem. Soc.* **1997**, *119*, 2240-2248.
32. Shelimov, K. B.; Jarrold, M. F., *J. Am. Chem. Soc.* **1997**, *119*, 2987-2994.
33. Jurneczko, E.; Kalapothakis, J.; Campuzano, I. D. G.; Morris, M.; Barran, P. E., *Anal. Chem.* **2012**, *84* (20), 8524-8531.
34. Ahmed, A.; Cho, Y. J.; No, M.-h.; Koh, J.; Tomczyk, N.; Giles, K.; Yoo, J. S.; Kim, S., *Anal. Chem.* **2011**, *83* (1), 77-83.
35. Thomson, B. A., *J. Am. Soc. Mass Spectrom.* **1997**, *8*, 1053-1058.
36. Wyttenbach, T.; Bowers, M. T., *J. Phys. Chem. B* **2011**, *115*, 12266-12275.

37. Regis, W. C. B.; Fattori, J.; Santoro, M. M.; Jamin, M.; Ramos, C. H. I., *Arch. Biochem. Biophys.* **2005**, *436* (1), 168-177.

Chapter 3 - Protein Structural Studies by TWIMS: A Critical Look at ESI Sources and Molecular Dynamics Models

3.1 Introduction

The possibility to transfer proteins from solution into the gas phase by electrospray ionization (ESI)¹ or nanoESI² offers exciting opportunities for the characterization of these analytes by mass spectrometry (MS) and related techniques. Many studies suggest that under properly optimized “gentle” conditions native-like protein structures and interactions can be retained *in vacuo*.³⁻⁵ On the other hand, there are also reports of disparities between protein behavior in solution and in the gas phase.⁶⁻¹⁰ This ongoing dispute is rooted in the challenges associated with obtaining structural information on gaseous analytes. X-ray crystallography, NMR spectroscopy, and cryo-electron microscopy are only applicable in the condensed phase. In the future free electron lasers may provide atomically resolved images of solvent-free biomolecules,¹¹ but until then other approaches have to be used. These include spectroscopic tools,¹²⁻¹⁴ dissociation experiments,^{5-6,8} gas phase H/D exchange,¹⁵⁻¹⁶ soft landing/EM,^{4,17} and computer simulations.^{10, 18-20} At present, the technique that is most widely used for characterizing biomolecular conformations in the gas phase is ion mobility spectrometry (IMS).²¹⁻²⁷

IMS experiments on native proteins and noncovalent assemblies require gentle conditions, such that structural perturbations are minimized. The analytes are typically electrosprayed in

neutral aqueous solution. Potential gradients along the ion path have to be carefully optimized. Voltages that are too low provide inadequate desolvation and poor transmission.²⁸⁻²⁹ Conversely, voltages that are too high will disrupt intra- and intermolecular contacts via collisional heating. Thermally excited biomolecules can undergo collisional unfolding and/or collision-induced dissociation (CID).³⁰⁻³² Structural collapse may take place as well.^{9, 19, 33}

Two main options exist for converting solution phase proteins into gaseous ions. (i) Regular ESI operates at flow rates in the $\mu\text{L min}^{-1}$ range, using a metal emitter capillary.^{1, 34} (ii) NanoESI operates with capillaries that have a much narrower outlet, giving rise to smaller initial droplets, and flow rates of less than 100 nL min^{-1} .² Advantages of nanoESI include improved desolvation, greater salt tolerance, and higher ion yield.^{29, 35-36} However, nanoESI tends to be less robust in terms of signal stability and reproducibility than regular ESI.³⁷⁻³⁸ It is often implied that nanoESI is better suited for preserving protein-protein interactions.^{29, 39} It is claimed that the small initial droplets require reduced number and energy of the collisions to desolvate the analytes. Other support refers to the unnecessary use of organic solvents or high interface temperature which is not compatible to the native environment in the solution to aid desolvation and droplet fission process. However, experimental evidence suggests this not necessarily to be true.⁴⁰⁻⁴² A related question is whether nanoESI is better suited for IMS experiments that aim to preserve solution structures. Two recent investigations focused on gaseous ubiquitin. One of these studies employed regular ESI and concluded that the protein undergoes unfolding in the gas phase.⁶ The other study employed nanoESI and reported that ubiquitin retains a native-like structure.³ Although the experiments differed in other aspects as well, these opposing findings highlight the need to scrutinize whether biomolecular structures in the gas phase depend on the electrospray method used.

Molecular dynamics (MD) techniques describe complex chemical systems based on realistic atomic models derived from other techniques. The application helps accurately understanding and predicting structural and dynamic properties of molecules. MD simulations on proteins are introduced since computer technology is developing so fast that makes it possible to simulate folding events close to the reality. MD simulations rely on the *Newton's* equations:

$$m_i \times \mathbf{a}(\mathbf{r}_i) = \mathbf{F}_i, i = 1, 2, 3, \dots, N. \quad (3.1a)$$

$$m_i \frac{\partial^2 \mathbf{r}_i}{\partial t^2} = \mathbf{F}_i \quad (3.1b)$$

i refers to the coordinates of each atom. The force \mathbf{F}_i experienced by the atom is derived from its potential energy $V(\mathbf{r}_i)$. So that \mathbf{F}_i can also be described as:

$$\mathbf{F}_i = - \frac{dV(\mathbf{r}_i)}{d\mathbf{r}_i} \quad (3.2)$$

with the setting of required temperature and pressure, the velocity and position of each atom can be simulated after a certain time ($t_0 + \Delta t$), where Δt is a very small time increment:

$$\mathbf{v}_i(t_0 + \Delta t) = \mathbf{v}_i(t_0) + \mathbf{a}(\mathbf{r}_i) \times \Delta t \quad (3.3a)$$

$$\mathbf{r}_i(t_0 + \Delta t) = \mathbf{r}_i(t_0) + \mathbf{v}_i(t_0) \times \Delta t + \frac{1}{2} \mathbf{a}(\mathbf{r}_i) \times (\Delta t)^2 \quad (3.3b)$$

The coordinates $\mathbf{r}_i(t_0 + \Delta t)$ as a function of time therefore represent the trajectory of the system. However, there are some limitations. The use of *Newton's* law means the simulations adapt classical mechanics for all the motions of atoms. But there are some exceptions involved in quantum mechanical character such as the motion of hydrogen atoms and helium liquid.

Also, the definition of force field $V(r_i)$ is not always valid since it does not take account the polarizabilities and fine-tuning of bonded interactions.⁴³

In this work we conduct a detailed comparison of TWIMS experiments on a number of proteins under regular ESI and nanoESI conditions. Measured collision cross-sections are compared to crystal structures and MD-derived gas phase model structures.

3.2 Experimental

3.2.1 Sample Preparation

Bovine ubiquitin (Ubq, 8565 Da), horse heart cytochrome c (Cyt, 12359 Da), and equine holo-myoglobin (hMb, 17568 Da) were purchased from Sigma (St. Louis, MO). Hemoglobin (Hb, 64478 Da) was isolated from fresh bovine blood.⁴⁴ Native solutions were prepared in 10 mM aqueous ammonium acetate at a protein concentration of 10 μM (pH 7). For Hb the concentration was increased to 60 μM .

3.2.2 Instrument Settings

Measurements were conducted on a Synapt HDMS time-of-flight mass spectrometer (Waters, Milford, MA).⁴⁵⁻⁴⁶ Regular ESI-MS experiments employed the standard Z-spray source at a capillary voltage of 2.8 kV and a desolvation gas flow rate of 500 L h^{-1} . Solutions were infused at 5 $\mu\text{L min}^{-1}$. NanoESI was conducted using gold-coated emitters made from borosilicate glass capillaries (BF 100-78-10, Sutter, Novato, CA) using a microcapillary puller (Sutter PC-84). Capillaries were coated using a Hummer VI Sputtering System (Union City, CA) operated at

a N₂ plasma pressure of 100 mTorr and 10 mA for 5 minutes. The nanoESI source was operated at 1.5 kV and the flow was assisted with a N₂ pressure of 0.05 bar. The resulting flow rate was ~40 nL min⁻¹, as determined gravimetrically. The source (backing) pressure was adjusted to 5 mbar by a SpeediValve on the scroll pump. Regardless of the type of electrospray source, the following TWIG parameters were used. The extraction cone was set to 1 V, the cone gas flow rate was 50 L h⁻¹, while the source and desolvation temperatures were 25°C and 40 °C, respectively. The trap collision energy was 2 V, the trap wave velocity was 100 m s⁻¹ and trap wave height was 0.1 V. Trap bias values between 8 and 9 V were used for the different proteins to ensure manageable ion transmission. The IMS wave height was set to 6.5 V at 300 m s⁻¹. The transfer collision energy was 4 V at 247 m s⁻¹, and the transfer wave height was 4 V. Other instrument parameters were as follows: trap entrance 1 V, IMS entrance 6.7 V, IMS exit 0 V, transfer entrance 1 V, and transfer exit 1 V. The trap release time was 500 μs. TWIG pressures were 1.58 × 10⁻² mbar in the trap (corresponding to trap gas “off”), while 0.5 mbar N₂ served as IMS gas. It will be seen that these instrument settings provide very gentle conditions with a minimum of ion activation when used in combination with a low sample cone voltage (5 V). For collisional heating experiments the sample cone voltage was raised up to 100 V.

3.2.3 Molecular Dynamics Simulations

Vacuum MD simulations were conducted using GROMACS 4.6.5⁴⁷ with the CHARMM27 force field,⁴⁸ unless noted otherwise. All bonds were constrained, thereby allowing for a 2 fs time step. To take advantage of GPU acceleration a 1 μm periodic box was used with a 333.3 nm non-bonded interaction cut-off. X-ray structures 1UBQ, 1HRC, 1WLA, and 2QSS served as starting points, after removal of water and addition of hydrogens using PDB2GMX. Proteins

electrosprayed in positive ion mode may retain some salt bridges, implying that negative solution charge on selected Glu and Asp side chains can survive.⁴⁹ However, the high proton mobility in gaseous proteins,⁵⁰ along with the high proton affinity of Glu- and Asp- implies that most acidic side chains will adopt their neutral form.^{19, 51-53} For our simulations all Glu and Asp were therefore neutralized by protonation. Excess protons were assigned to Arg and Lys on the protein surface, providing approximately equidistant charge spacing and net charge values consistent with the experiments. CHARMM force fields do not provide parameters for neutral heme propionates; those sites were therefore negatively charged. This was compensated by protonation of adjacent Arg and/or Lys. Cyt simulations employed a customized script and a slightly modified version of the CHARMM36 force field⁴⁸ which allowed for proper parametrization of heme c,⁵⁴ axial iron ligation, thioether bonds between heme and Cys14/Cys17, as well as the presence of several non-protonated Lys. Production runs were conducted at 300 K for 40 ns with Nosé-Hoover thermalization⁵⁵ to mimic the presence of blackbody radiation and background gas.

MOBCAL was used for calculating He Ω values.⁵⁶⁻⁵⁷ X-ray data for MOBCAL analyses were processed analogously to MD starting structures. Several algorithms are available for predicting Ω values of model structures. The projection approximation yields values that are too low. The exact hard sphere scattering (EHSS) algorithm produces values that are more reliable, within ~1% of those generated by the trajectory method.¹⁸ The low computational cost of the EHSS algorithm has made it the method of choice for many practitioners.^{3, 18, 23, 58} We will thus base our considerations on calculated Ω_{EHSS} values.

3.3 Results and Discussion

3.3.1 Instrument-to-Instrument Reproducibility

For testing the consistency of TWIMS data across different laboratories we examined Cyt at pH 3. Experimental conditions were chosen to match those of an earlier study⁵⁹ that employed the same instrument type as the one used here (see Figure 3-1 caption for details). The TWIMS profile obtained for Cyt 8+ shows a major signal at 8.7 ms, and a minor feature at 12.3 ms (Figure 3-1A). These data are almost identical to those displayed in Figure 3-1B of ref.⁵⁹ Similar agreement was observed for other charge states (not shown). These observations demonstrate that the TWIMS platform yields data that are highly reproducible.

Notwithstanding the robustness of the instrumentation, the data obtained depend critically on the parameters used. Figure 3-1B demonstrates the effects of lowering the sample cone voltage and trap collision energy. The TWIMS profile obtained under these conditions is shifted to 4.7 ms, corresponding to a more compact protein structure than in Figure 3-1A. These observations suggest that the settings used for Figure 3-1A induce collisional unfolding,³⁰⁻³² whereas the conditions of Figure 3-1B are gentler. We cannot rule out that some collisional unfolding still takes place with these softer settings, because cone voltages below 5 V lead to loss of signal. This uncertainty regarding the absolute level of ion activation introduces challenges for the instrument calibration, as outlined in the subsequent section.

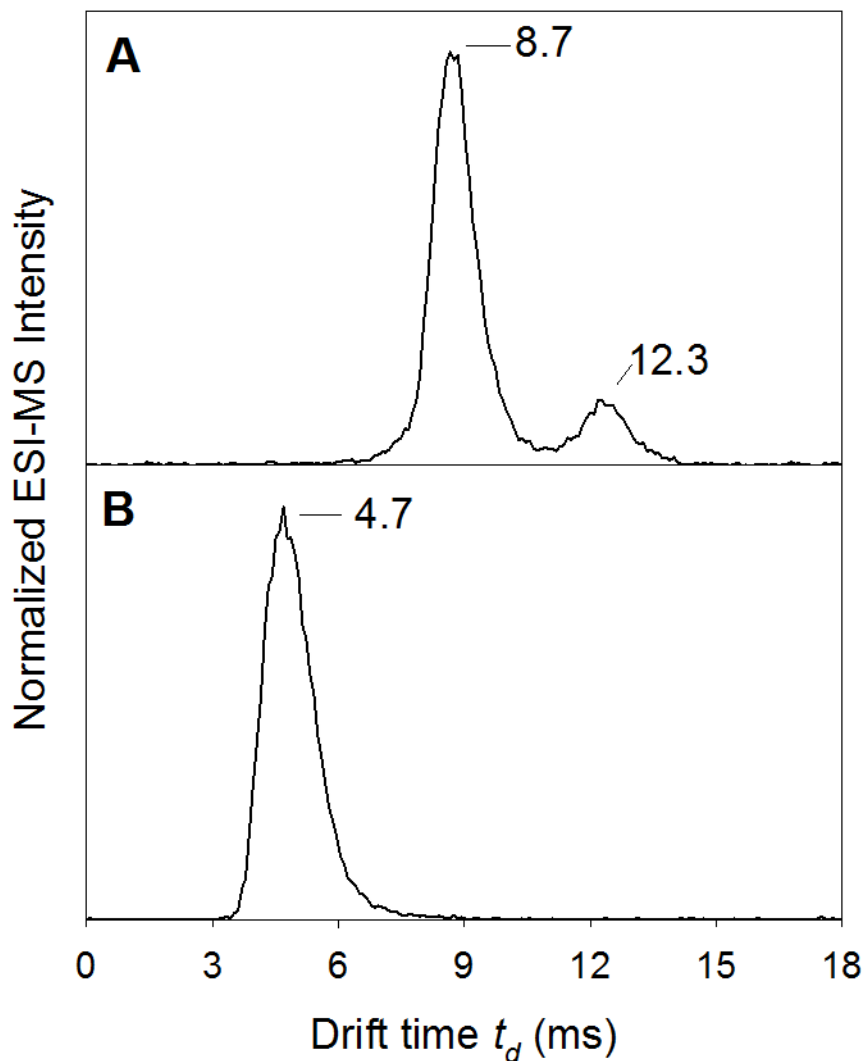


Figure 3-1 TWIMS profile for Cyt 8+ at pH 3.

It is recorded with (A) sample cone voltage 75 V, trap collision energy 5 V, transfer collision energy 3 V; (B) cone voltage 5 V, trap collision energy 2 V, transfer collision energy 4 V. Common conditions for both data sets: 50 mM ammonium acetate solution acidified with formic acid to pH 3; regular ESI source at 10 $\mu\text{L min}^{-1}$; source temperature 80 $^{\circ}\text{C}$; desolvation temperature 150 $^{\circ}\text{C}$; IM T-wave velocity 300 m s^{-1} with a 6.6 V wave height; transfer wave velocity 300 m s^{-1} with a 3 V wave height.

3.3.2 TWIMS of Native Proteins Using Regular ESI and nanoESI

Older drift tube investigations generally used regular ESI, whereas recent IMS studies predominantly employed nanoESI. Given the purported “softness advantage” of nanoESI,^{29, 39} we set out to examine if the properties of gaseous Ubq, Cyt, hMb, and Hb depend on the type of electrospray source. In contrast to the calibrant mix, the neutral aqueous solvent employed for the subsequent measurements ensures native conformations in bulk solution. Also, a cone voltage of 5 V was used to minimize collisional activation. All other voltages along the ion path were minimized as well (see Methods for details). Mass spectra obtained under these conditions are dominated by low charge states (Figure 3-2).⁶⁰ A lack of heme loss from hMb,⁶¹ as well as the dominance of intact Hb tetramers^{42, 58} confirm the gentle nature of the experiments. Consistent with recent reports,⁴² very similar charge state distributions were obtained for nanoESI and regular ESI. However, salt adduction was less pronounced for nanoESI.^{29, 35-36}

TWIMS profiles acquired under gentle conditions display well-resolved maxima, corresponding to Ω values of 986 Å² for Ubq, 1351 Å² for Cyt, 1782 Å² for hMb, and 4552 Å² for Hb (Figure 3-3). These results agree with experimental literature values to within 2% or better.^{3, 18, 58, 62} Most importantly, Figure 3-3 demonstrates that virtually identical data are obtained when employing regular ESI or nanoESI.

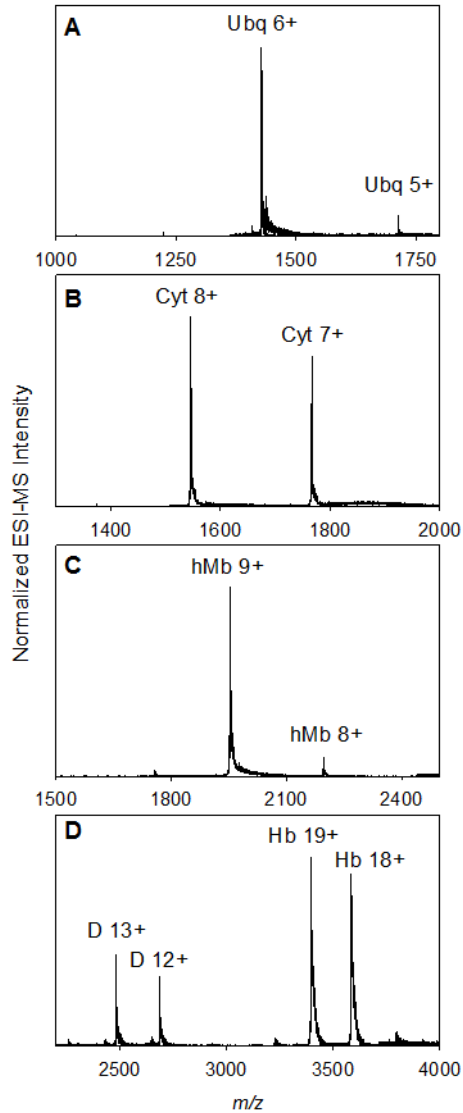


Figure 3-2 Mass spectra of four proteins under gentle conditions

(A) Ubq, (B) Cyt, (C) hMb and (D) Hb generated using nanoESI under native solution conditions. The sample cone was set to 5 V to minimize collisional heating. “Hb” in panel D refers to $\alpha_2\beta_2$, whereas “D” refers to $\alpha\beta$ dimers that arise from the natural dissociation equilibrium of the protein in solution.⁴²

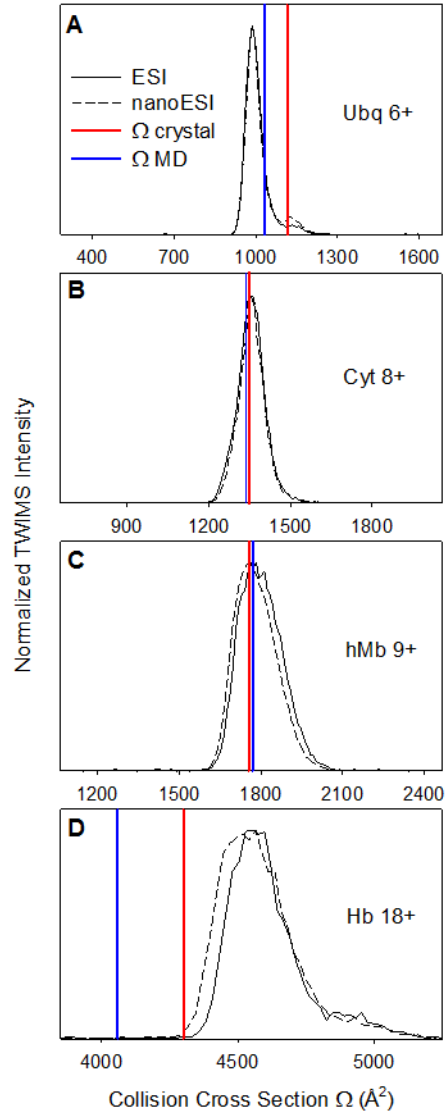


Figure 3-3 Calibrated TWIMS data for four proteins under native condition.

(A) Ubq 6+, (B) Cyt 8+, (C) hMb 9+ and (D) Hb 18+ electrosprayed in neutral aqueous solution using gentle source conditions (sample cone 5 V). Each panel compares two data sets that were obtained using regular ESI (solid black lines) and nanoESI (dashed black lines). Red vertical lines indicate crystal structure Ω_{EHSS} values. Blue vertical lines represent average Ω_{EHSS} values obtained from the 21-40 ns range of gas phase MD simulations.

To explore possible differences in the internal energy of protein ions produced by the two electrospray techniques we performed collisional unfolding measurements. The rationale behind these experiments is that conformational changes of gaseous ions involve thermally activated barrier crossing.³² Collisional heating of ions with dissimilar internal energy should thus lead to different unfolding profiles. Analyte activation can be achieved at several points along the ion path.^{45-46, 63-64} We chose to focus on the sample cone because it is the element closest to the electrospray source. TWIMS analyses were conducted at cone voltages ranging from 5 V to 100 V (Figure 3-4). Average collision cross sections Ω_{av} were then calculated as

$$\Omega_{av} = \frac{\int I(\Omega)\Omega d\Omega}{\int I(\Omega) d\Omega} \quad (3.4)$$

The data obtained in this way (Figure 3-5) reveal the prevalence of compact gas phase structures for low excitation energies, whereas more extended conformers dominate for cone voltages of 90-100 V. The Ω increase is monotonic for Ubq, Cyt, and hMb (Figure 3-5A-C). The Hb profiles show a dip between 20 V and 60 V, before unfolding takes place at higher voltages (Figure 3-5D). This dip reflects a gas phase compaction process that has previously been reported for Hb³³ and some other complexes.^{9, 19} The key conclusion from the data of Figure 3-5 is that ions produced by regular ESI and nanoESI exhibit virtually the same collisional unfolding profiles. This implies that the internal energy of the ions must be very similar for both electrospray techniques.

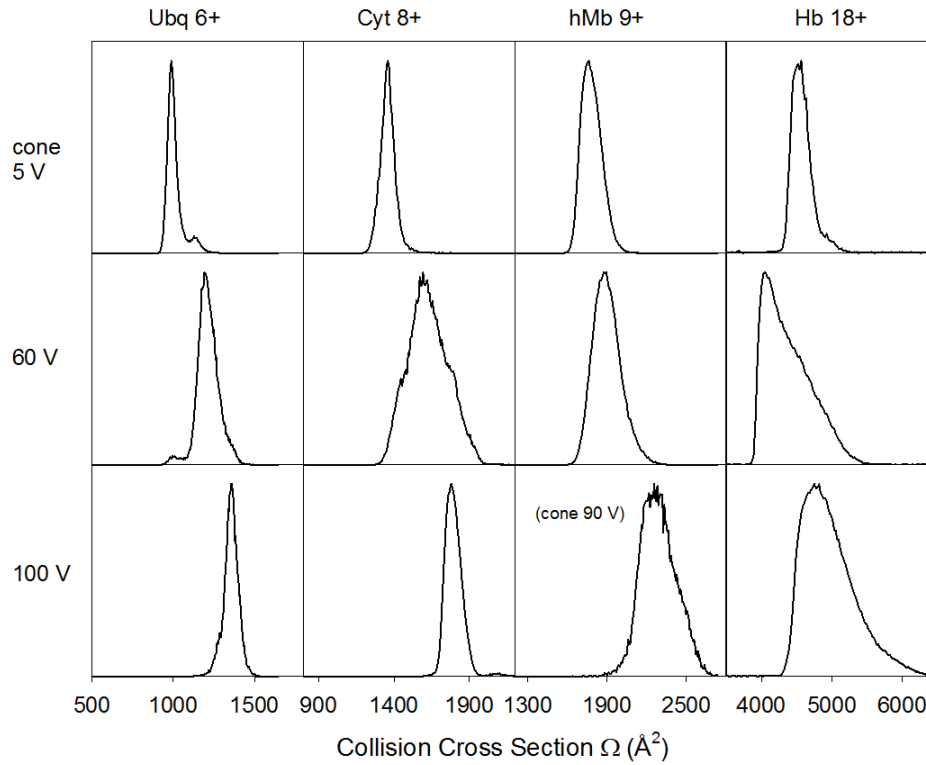


Figure 3-4 Calibrated TWIMS profiles for the ion species noted along the top.

Ions were produced by nanoESI under native solution conditions. Data were acquired with different sample cone settings, as noted on the left. In the case of hMb experiments at a sample cone voltage of 100 V were not feasible due to collisional heme loss, thus the highest value used was 90 V.

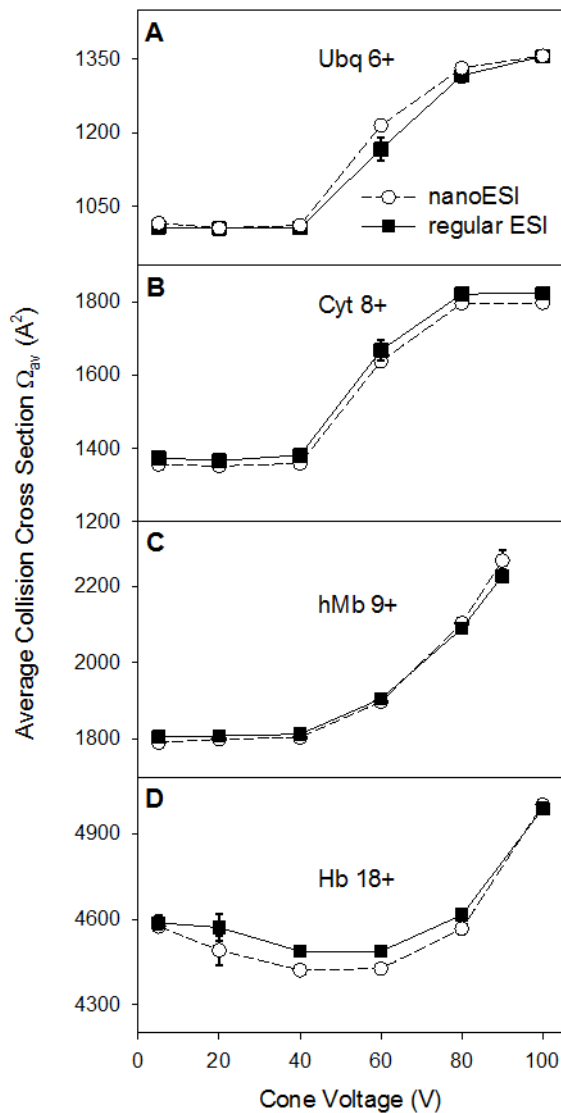


Figure 3-5 Average collision cross sections Ω_{av} as a function of cone voltage.

(A) Ubq 6+, (B) Cyt 8+, (C) hMb 9+ and (D) Hb 18+. Each panel show two data sets; open circles refer to nanoESI experiments, filled squares were measured using regular ESI.

3.3.3 X-ray Structure and MD Conformation

Vacuum MD data were generated using charge states that matched the experimental values. Root mean square deviation (RMSD) describes the deviation of the MD simulated structure ($r_i(t_2)$) from the reference structure ($r_i(t_1)$, $t_1 = 0$) which is derived from X-ray diffraction experiment in this work:

$$\text{RMSD}(t_1, t_2) = \left[\frac{1}{M} \sum_{i=1}^N m_i \|r_i(t_1) - r_i(t_2)\|^2 \right]^{\frac{1}{2}} \quad (3.5)$$

where $M = \sum_{i=1}^N m_i$ and $r_i(t)$ is the coordinate of atom i at time t . The analyses reveal some rearrangements early during the runs, but RMSDs then stabilize and remain quite steady after ~ 20 ns (Figure 3-6). This suggests that the ions have settled into metastable conformations at this time.²⁰ In the following we will focus on MD data obtained in the 20-40 ns range. RMSDs around 3 Å are seen for Ubq, Cyt, and hMb. Deviations from the crystal structure are more pronounced for Hb, with $\text{RMSD} \approx 4$ Å. The small deviations indicate that the MD structure is similar to the X-ray structure to a large extent. However, RMSD is not quite accurate to perform the differences between these two structures since it introduces absolute value.

A useful parameter for characterizing MD structures is the radius of gyration

$$R_g = \left(\frac{\sum_i (r_i^2 m_i)}{\sum_i m_i} \right)^{1/2} \quad (3.6)$$

where m_i is the atomic mass of atom i , and r_i is the corresponding distance from the center of mass. R_g depicts the compactness of the proteins. Positive and negative deviations represent the more stretched and more compact structures respectively. Both R_g and Ω report on the overall protein compactness, although it is not easy to establish a direct relationship between

the two parameters.⁶¹ We separately computed R_g for the whole protein, the backbone, and the side chains (Figure 3-7). Average R_g values are summarized in Figure 3-8, along with overlays of the crystal structures (red) and the $t = 40$ ns MD conformations (blue). Comparison of the MD vs. X-ray structures of Ubq, Cyt, and hMb reveals only relatively minor conformational changes (Figure 3-8A-C). A slight decrease in R_g is seen for Ubq, mainly reflecting a collapse of the extended C-terminal tail towards the protein surface (Figure 3-8A). Cyt exhibits a small R_g increase as the N-terminal helix adopts an ajar orientation (Figure 3-8B). R_g also increases slightly for hMb, reflecting some changes in the termini and other minor rearrangements (Figure 3-8C). The largest conformational change takes place for Hb, where R_g decreases by almost 5%. This compaction reflects a shift of several helices towards the central cavity of the tetramer, similar to events seen in simulations on other protein complexes.¹⁹ Overall, the MD results of Figure 3-8 nonetheless suggest that all four gaseous proteins retain much of their condensed phase structure. This finding is consistent with earlier simulations.^{10, 18-20}

Based on the R_g data of Figure 3-8 one can scrutinize the commonly made claim that side chains will collapse onto the surface of gaseous proteins.^{3, 20, 23, 65} The side chains are considered to be rearranged in the vacuum MD simulations, so that hydrophilic residues no longer interact with solvent, instead, interact with each other. Therefore, the salt bridges and charge-dipole interactions occur and lead to the collapse. The slight compaction of Ubq relative to the X-ray data is caused mainly by rearrangements of the backbone, whereas the side chain R_g remains almost unchanged (Figure 3-8A). Cyt shows a subtle expansion that originates mainly from backbone movements (Figure 3-8B). The small expansion of hMb has both backbone and side chain contributions (Figure 3-8C). Hb compaction originates from movements of both backbone and side chains (Figure 3-8D). Thus, our MD data do not show

a large-scale collapse of side chains onto the protein surface. Earlier evidence for such a collapse comes from simulations that employed solution charges on side chains (Arg⁺, Lys⁺, Glu⁻, Asp⁻).²⁰ Such arrangements cause mutual attraction and favor the formation of salt bridges. As noted in the Methods section, our simulations employed a different approach with neutral Asp and Glu (along with Arg⁺ and Lys⁺), which is thought to describe the behavior of gaseous proteins more adequately.^{19, 51-53} Side chain collapse is not favored under these conditions because extensive salt bridges will not form and because Arg⁺ / Lys⁺ moieties experience mutual repulsion.

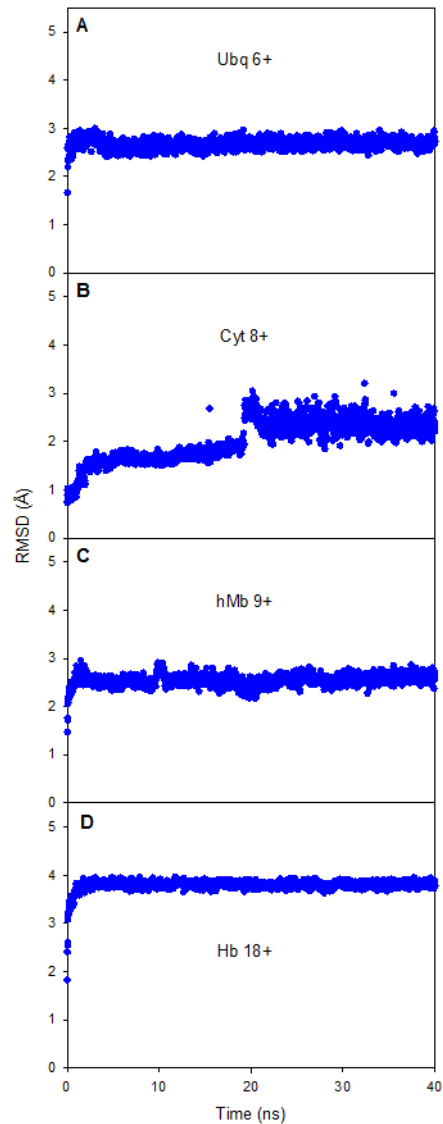


Figure 3-6 Root mean square deviation (RMSD) of the four model proteins.

The RMSD is relative to the corresponding X-ray crystal starting structures throughout the 40 ns MD simulation time window. The data were calculated on the basis of C_{α} coordinates. An RMSD value of zero would correspond to a conformation that is identical to the X-ray structure. The transition seen for Cyt at $t \approx 19$ ns originates from “opening” of the N-terminal helix

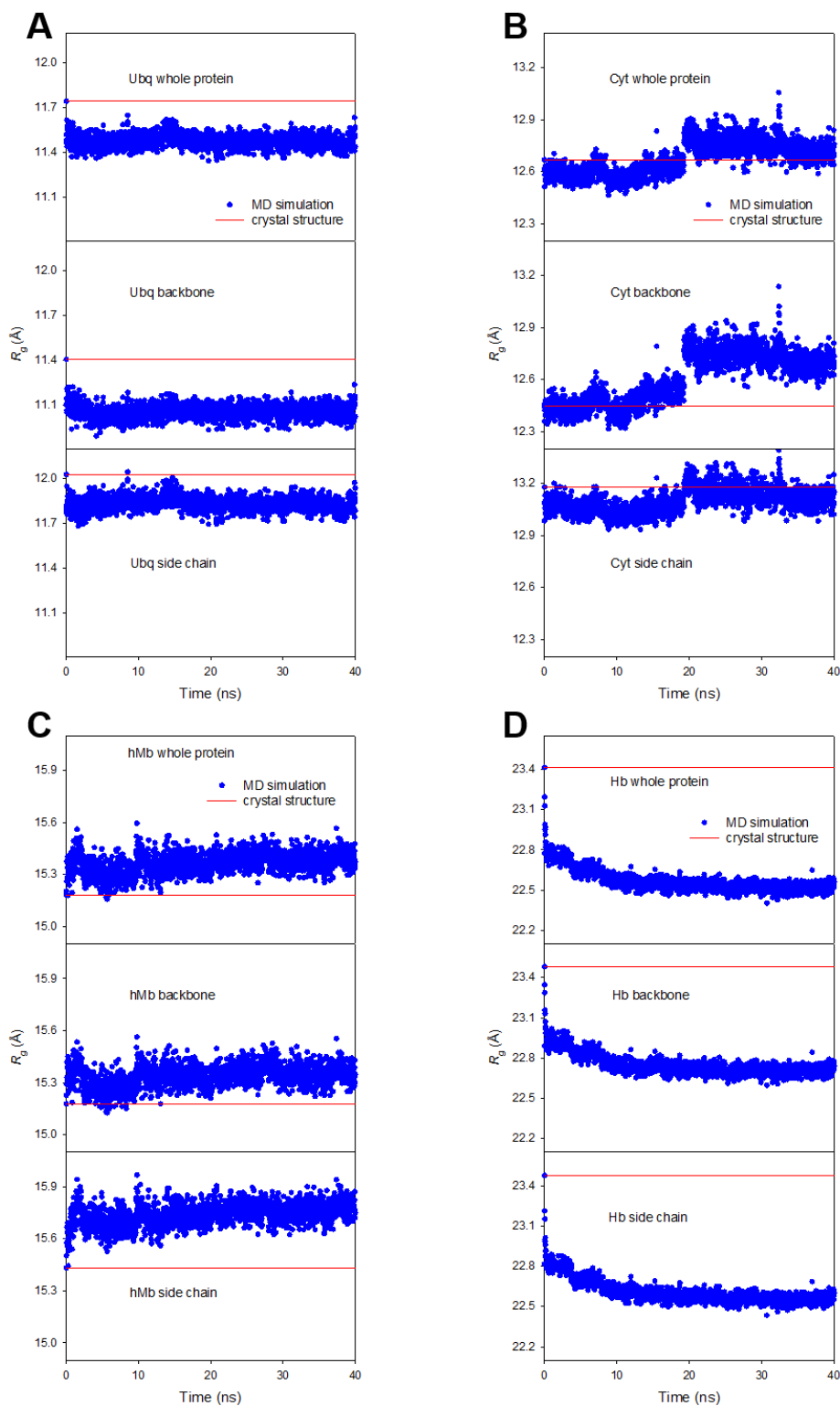


Figure 3-7. Radius of gyration (R_g) of four proteins.

R_g is calculated throughout the 40 ns MD trajectories of (A) Ubq 6+, (B) Cyt 8+, (C) hMb 9+, and (D) Hb 18+. Three panels are shown for each protein ion, corresponding to R_g of the whole protein, backbone atoms only, and side chain atoms only (top to bottom).

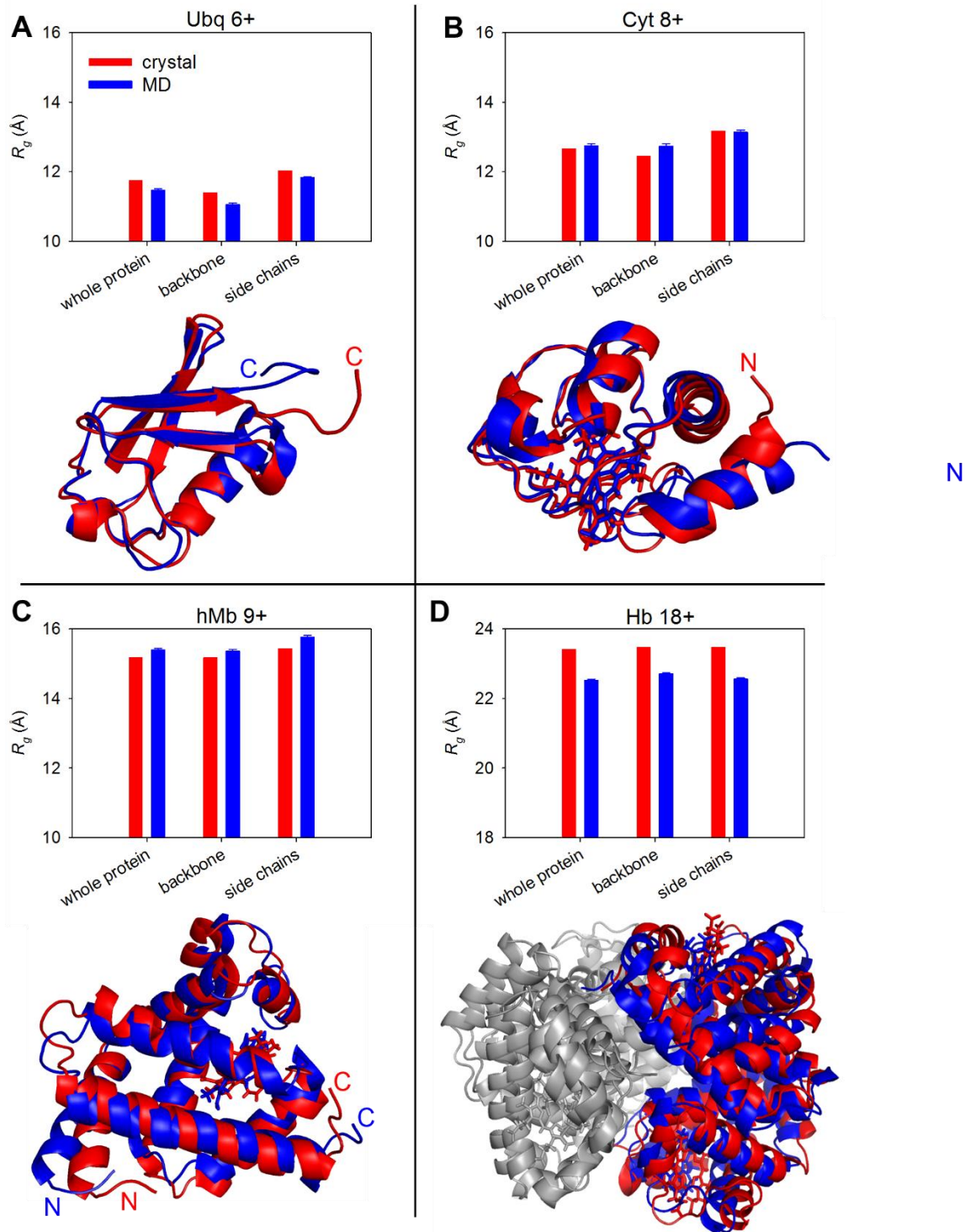


Figure 3-8 Comparison of crystal structures (red) and MD simulation results for $t = 40$ ns (blue).

Data are shown for (A) Ubq 6+, (B) Cyt 8+, (C) hMb 9+ and (D) Hb 18+. Also shown in each panel is the radius of gyration R_g of the crystal structures and the MD conformations. R_g was determined separately for the whole protein, the backbone, and the side chains. In panel D one pair of Hb $\alpha\beta$ subunits is shown in gray to simplify the graphics.

3.3.4 Comparison of TWIMS Data with MD-Derived and Crystallographic Ω_{EHSS} Values

Crystal and MD structures share virtually the same Ω_{EHSS} values for both Cyt and hMb. It is gratifying that these values also agree with the experimental TWIMS cross sections to within ~1% (Figure 3-3B, C). Ω_{EHSS} of the Ubq MD conformation is ~8% smaller than that of the crystal structure (Figure 3-3A). This difference mainly reflects the collapse of the Ubq C-terminus, as noted in Figure 3-8A. The MD-derived Ω_{EHSS} is only 4% different from the measured TWIMS cross section (Figure 3-3A). Taking into account the ongoing discussion regarding the accuracy of calculated Ω values,^{9, 66} the agreement between MD models and experiments in Figure 3-3A-C is quite remarkable. This agreement supports the view that, at least for some proteins, solution structure can be largely retained in the gas phase.³⁻⁵

Interestingly, the Ubq TWIMS profile displays a small feature that coincides with Ω_{EHSS} of the crystal structure (Figure 3-3A, red line). It is tempting to speculate that this feature might represent a gas phase conformer with an extended C-terminal tail, similar to the crystal conformation (Figure 3-8A, red). As noted earlier, the dominant peak in Figure 3-3A represents a more compact structure, likely with a collapsed C-terminus as in the MD structure (Figure 3-8A, blue).

The experimental Ω value of Hb is 5% larger than Ω_{EHSS} of the crystal structure. It is unlikely that this mismatch reflects a calibration artifact because (i) the t_d of Hb is well within the range covered by calibrant ions and (ii) the measured Ω agrees closely with the literature.⁵⁸ In contrast to the monomeric proteins discussed above, Hb therefore appears to be slightly more expanded in the gas phase than in the crystal. A substantial mismatch (11%) is seen when

comparing the experimental Ω value to Ω_{EHSS} of the MD conformation (Figure 3-3D). This increased difference arises from Hb compaction taking place during the MD simulation (Figure 3-8D). It thus appears that the MD conformation of Figure 3-8D does not represent a good structural model of Hb ions generated under the experimental conditions of Figure 3-3D. Instead, electrospray with these gentle instrument settings (sample cone 5 V) produces ions with Ω values that are closer to Ω_{EHSS} of the crystal structure. It is possible that the collapsed Hb MD structure resembles the compacted species seen after moderate collisional activation³³ (Figure 3-5D). Additional investigations of this interesting issue are currently ongoing in our laboratory.

3.4 Conclusions

Like most previous studies, this work assumes that simple approaches such as the EHSS method⁵⁶⁻⁵⁷ can predict Ω values of model structures with reasonable accuracy. While acknowledging the limitations of such algorithms,^{9, 66-67} we hope that future work will show systematic errors to be small.

The MD data of this work indicate the absence of a major side chain collapse, which has previously been assumed to be a general feature of electrosprayed protein ions.^{3, 20, 23, 65} MD conformations of Ubq, Cyt, and hMb are in good agreement with experimental TWIMS data. In the case of Hb the MD structure is more compact than the experimentally observed ions. Instead, electrosprayed Hb appears to have a conformation closer to the X-ray structure. This demonstrates that gentle instrument settings (sample cone = 5 V) and “gentle MD conditions” (T = 300 K) do not necessarily produce gas phase structures that are consistent with each other. Simple vacuum MD simulations, therefore, may not always provide improved candidate

structures for the interpretation of TWIMS data. This situation will likely improve when using MD strategies that reflect the ion “history” including its release from electrospray droplets, rather than just exposing proteins to a vacuum environment at the onset of the simulation.

Overall, our data support the view³⁻⁵ that gaseous proteins can get kinetically trapped in solution-like conformations.⁶⁸⁻⁶⁹ Retention of solution structure in electrospray experiments on native proteins is promoted by the low charge states of the corresponding ions.⁶⁰ A different situation is encountered for proteins that adopt semi-unfolded conformations in bulk solution. The highly charged ions formed under such conditions experience rapid loss of structure as a result of their large internal Coulomb repulsion.^{3, 7, 42}

In an earlier study we demonstrated that regular ESI maintains noncovalent protein-protein contacts at least as well as nanoESI.⁴² Similarly, the findings reported here reveal no difference for ions produced by regular ESI or nanoESI (Figures 3-3, 3-5). *Wytembach et al.*³ reported that nanoESI produces native-like Ubq ions. In contrast, *Skinner et al.*⁶ employed regular ESI and found that Ubq unfolds in the gas phase. We have no reason to doubt the findings of either study. The current work implies that the different results obtained in those two earlier investigations^{3, 6} are not related to the electrospray technique used. Instead, the opposing results likely originate from the extended ion storage time (seconds) used in ref.⁶ which increases the likelihood of conformational transitions. In contrast, the millisecond time frame of TWIMS and drift tube IMS (as in ref.³) favors the observation of metastable conformers that maintain solution properties for a relatively short interval after being released into the vacuum.

It is concluded that the application of IMS to natively folded proteins represents a viable structural biology tool. We nonetheless encourage practitioners to always approach their own

data (and those of others) with a healthy dose of skepticism. Ultimately, this will help the acceptance of gas phase techniques by the wider condensed phase community.

3.5 References

1. Fenn, J. B., *Angew. Chem. Int. Ed.* **2003**, *42*, 3871-3894.
2. Wilm, M.; Mann, M., *Anal. Chem.* **1996**, *68*, 1-8.
3. Wytttenbach, T.; Bowers, M. T., *J. Phys. Chem. B* **2011**, *115*, 12266-12275.
4. Mikhailov, V. A.; Mize, T. H.; Benesch, J. L. P.; Robinson, C. V., *Anal. Chem.* **2014**, *86* (16), 8321-8328.
5. Liu, L.; Bagal, D.; Kitova, E. N.; Schnier, P. D.; Klassen, J. S., *J. Am. Chem. Soc.* **2009**, *131*, 15980-15981.
6. Skinner, O. S.; McLafferty, F. W.; Breuker, K., *J. Am. Soc. Mass Spectrom.* **2012**, *23*, 1011-1014.
7. Vahidi, S.; Stocks, B. B.; Konermann, L., *Anal. Chem.* **2013**, *85* (21), 10471-8.
8. Ly, T.; Julian, R. R., *J. Am. Chem. Soc.* **2010**, *132*, 8602-8609.
9. Hogan, C. J.; Ruotolo, B. T.; Robinson, C. V.; de la Mora, J. F., *J. Phys. Chem. B* **2011**, *115* (13), 3614-3621.
10. Patriksson, A.; Marklund, E.; van der Spoel, D., *Biochemistry* **2007**, *46*, 933-945.
11. Bogan, M. J., *Anal. Chem.* **2013**, *85* (7), 3464-3471.
12. Talbot, F. O.; Rullo, A.; Yao, H.; Jockusch, R. A., *J. Am. Chem. Soc.* **2010**, *132*, 16156-16164.
13. Polfer, N. C.; Oomens, J., *Phys. Chem. Chem. Phys.* **2007**, *9*, 3804-3817.

14. Nagornova, N. S.; Guglielmi, M.; Doemer, M.; Tavernelli, I.; Rothlisberger, U.; Rizzo, T. R.; Boyarkin, O. V., *Angew. Chem. Int. Ed.* **2011**, *50*, 5383-5386.
15. Mistarz, U. H.; Brown, J. M.; Haselmann, K. F.; Rand, K. D., *Anal. Chem.* **2014**, *86* (23), 11868-11876.
16. Donohoe, G. C.; Khakinejad, M.; Valentine, S. J., *J. Am. Soc. Mass Spectrom.* **2015**, *26*, 564-576.
17. Siuzdak, G.; Bothner, B.; Yeager, M.; Brugidou, C.; Fauquet, C. M.; Hoey, K.; Chang, C. M., *Chem. Biol.* **1996**, *3*, 45-48.
18. Mao, Y.; Woenckhaus, J.; Kolafa, J.; Ratner, M. A.; Jarrold, M. F., *J. Am. Chem. Soc.* **1999**, *121* (12), 2712-2721.
19. Hall, Z.; Politis, A.; Bush, M. F.; Smith, L. J.; Robinson, C. V., *J. Am. Chem. Soc.* **2012**, *134*, 3429-3438.
20. Steinberg, M. Z.; Elber, R.; McLafferty, F. W.; Gerber, R. B.; Breuker, K., *ChemBioChem* **2008**, *9*, 2417-2423.
21. May, J. C.; McLean, J. A., *Anal. Chem.* **2015**, *87* (3), 1422-1436.
22. Konijnenberg, A.; Butterer, A.; Sobott, F., *Biochim. Biophys. Acta* **2013**, *1834* (6), 1239-1256.
23. Jurneckzo, E.; Barran, P. E., *Analyst* **2011**, *136*, 20-28.
24. Utrecht, C.; Rose, R. J.; van Duijn, E.; Lorenzen, K.; Heck, A. J. R., *Chem. Soc. Rev.* **2010**, *39* (5), 1633-1655.
25. Smith, D. P.; Knapman, T. W.; Campuzano, I.; Malham, R. W.; Berryman, J. T.; Radford, S. E.; Ashcroft, A. E., *European journal of mass spectrometry* **2009**, *15* (2), 113-30.

26. Silveira, J. A.; Servage, K. A.; Gamage, C. M.; Russell, D. H., *J. Phys. Chem. A* **2013**, *117* (5), 953-961.
27. Lee, J. W.; Kim, H. I., *Analyst* **2015**, *140* (2), 661-669.
28. Bush, M. F.; Hall, Z.; Giles, K.; Hoyes, J.; Robinson, C. V.; Ruotolo, B. T., *Anal. Chem.* **2010**, *82*, 9667-9565.
29. Benesch, J. L. P.; Ruotolo, B. T.; Simmons, D. A.; Robinson, C. V., *Chem. Rev.* **2007**, *107*, 3544-3567.
30. Valentine, S. J.; Counterman, A. E.; Clemmer, D. E., *J. Am. Soc. Mass Spectrom.* **1997**, *8* (9), 954-961.
31. Shelimov, K. B.; Clemmer, D. E.; Hudgins, R. R.; Jarrold, M. F., *J. Am. Chem. Soc.* **1997**, *119*, 2240-2248.
32. Shelimov, K. B.; Jarrold, M. F., *J. Am. Chem. Soc.* **1997**, *119*, 2987-2994.
33. Michaelevski, I.; Eisenstein, M.; Sharon, M., *Anal. Chem.* **2010**, *82*, 9484-9491.
34. Covey, T. R.; Thomson, B. A.; Schneider, B. B., *Mass Spectrom. Rev.* **2009**, *28*, 870-897.
35. Juraschek, R.; Dulcks, T.; Karas, M., *J. Am. Soc. Mass Spectrom.* **1999**, *10*, 300-308.
36. Marginean, I.; Page, J. S.; Tolmachev, A. V.; Tang, K. Q.; Smith, R. D., *Anal. Chem.* **2010**, *82*, 9344-9349.
37. Bovet, C.; Wortmann, A.; Eiler, S.; Granger, F.; Ruff, M.; Gerrits, B.; Moras, D.; Zenobi, R., *Protein Sci.* **2007**, *16* (5), 938-946.

38. Gabelica, V.; Vreuls, C.; Filee, P.; Duval, V.; Joris, B.; De Pauw, E., *Rapid Commun. Mass Spectrom.* **2002**, *16*, 1723-1728.
39. Hilton, G. R.; Benesch, J. L. P., *J. R. Soc. Interface* **2012**, *9*, 801-816.
40. Jecklin, M. C.; Touboul, D.; Bovet, C.; Wortmann, A.; Zenobi, R., *J. Am. Soc. Mass Spectrom.* **2008**, *19*, 332-343.
41. Loo, J. A., *Int. J. Mass Spectrom.* **2000**, *200*, 175-186.
42. Liu, J.; Konermann, L., *J. Am. Soc. Mass Spectrom.* **2011**, *22*, 408-417.
43. Van Gunsteren, W. F.; Karplus, M., *Macromolecules* **1982**, *15* (6), 1528-1544.
44. Boys, B. L.; Kuprowski, M. C.; Konermann, L., *Biochemistry* **2007**, *46*, 10675-10684.
45. Giles, K.; Pringle, S. D.; Worthington, K. R.; Little, D.; Wildgoose, J. L.; Bateman, R. H., *Rapid communications in mass spectrometry : RCM* **2004**, *18* (20), 2401-14.
46. Pringle, S. D.; Giles, K.; Wildgoose, J. L.; Williams, J. P.; Slade, S. E.; Thalassinou, K.; Bateman, R. H.; Bowers, M. T.; Scrivens, J. H., *Int. J. Mass Spectrom.* **2007**, *261*, 1-12.
47. Hess, B.; Kutzner, C.; van der Spoel, D.; Lindahl, E., *J. Chem. Theory Comput.* **2008**, *4*, 435-447.
48. Vanommeslaeghe, K.; Hatcher, E.; Acharya, C.; Kundu, S.; Zhong, S.; Shim, J.; Darian, E.; Guvench, O.; Lopes, P.; Vorobyov, I., *J. Comp. Chem.* **2010**, *31* (4), 671-690.
49. Marchese, R.; Grandori, R.; Carloni, R.; Raugei, S., *J. Am. Soc. Mass Spectrom.* **2012**, *23*, 1903-1910.
50. Boyd, R. K.; Somogyi, Á., *J. Am. Soc. Mass Spectrom.* **2010**, *21*, 1275-1278.

51. Schnier, P. D.; Gross, D. S.; Williams, E. R., *J. Am. Chem. Soc.* **1995**, *117* (25), 6747-6757.
52. Mao, Y.; Ratner, M. A.; Jarrold, M. F., *J. Phys. Chem. B* **1999**, *103*, 10017-10021.
53. Fegan, S. K.; Thachuk, M., *J. Chem. Theory Comput.* **2013**, *9* (6), 2531-2539.
54. Autenrieth, F.; Tajkhorshid, E.; Baudry, J.; Luthey-Schulten, Z., *J. Comput. Chem.* **2004**, *25* (13), 1613-1622.
55. Hoover, W. G., *Phys. Rev. A* **1985**, *31*, 1695-1697.
56. Mesleh, M. F.; Hunter, J. M.; Shvartsburg, A. A.; Schatz, G. C.; Jarrold, M. F., *J. Phys. Chem.* **1996**, *100* (40), 16082-16086.
57. Shvartsburg, A. A.; Jarrold, M. F., *Chem. Phys. Lett.* **1996**, *261* (1-2), 86-91.
58. Scarff, C. A.; Patel, V. J.; Thalassinou, K.; Scrivens, J. H., *J. Am. Soc. Mass Spectrom.* **2009**, *20*, 625-631.
59. Smith, D. P.; Giles, K.; Bateman, R. H.; Radford, S. E.; Ashcroft, A. E., *J. Am. Soc. Mass Spectrom.* **2007**, *18*, 2180-2190.
60. Dobo, A.; Kaltashov, I. A., *Anal. Chem.* **2001**, *73*, 4763-4773.
61. Collings, B. A.; Douglas, D. J., *J. Am. Chem. Soc.* **1996**, *118*, 4488-4489.
62. Hopper, J. T. S.; Oldham, N. J., *J. Am. Soc. Mass Spectrom.* **2009**, *20*, 1851-1858.
63. Ruotolo, B. T.; Benesch, J. L. P.; Sandercock, A. M.; Hyung, S.-J.; Robinson, C. V., *Nat. Protocols* **2008**, *3*, 1139-1152.

64. Taverner, T.; Hernandez, H.; Sharon, M.; Ruotolo, B. T.; Matak-Vinkovic, D.; Devos, D.; Russell, R. B.; Robinson, C. V., *Acc. Chem. Res.* **2008**, *41*, 617-627.
65. Warnke, S.; von Helden, G.; Pagel, K., *J. Am. Chem. Soc.* **2013**, *135* (4), 1177-1180.
66. Wyttenbach, T.; Bleiholder, C.; Bowers, M. T., *Anal. Chem.* **2013**, *85* (4), 2191-2199.
67. Larriba-Andaluz, C.; Hogan, C. J., *J. Chem. Phys.* **2014**, *141* (19).
68. van der Spoel, D.; Marklund, E. G.; Larsson, D. S. D.; Caleman, C., *Macromol. Biosci.* **2011**, *11*, 50-59.
69. Clemmer, D. E.; Valentine, S. J., *Nat. Chem.* **2009**, *1*, 257-258.

Chapter 4 - Conclusions

4.1 Conclusions and Future Work

Protein studies have involved many aspects including protein conformations, protein dynamics, and protein-protein interactions. A variety of biophysical techniques have been applied to study these and other aspects of proteins. Optical probes¹⁻³ provide protein structural information on a global scale. X-ray crystallography⁴ achieves success in determining crystal structure of proteins. Nuclear Magnetic Resonance (NMR) spectroscopy⁵ can complement X-ray analysis by providing insights into dynamic aspects of protein structure. In this work, we employed ESI-MS to monitor the conformation of proteins in the gas phase. ESI-MS is widely used in protein studying field results from its high sensitivity and its compatibility with other techniques, which makes it a powerful tool to study protein structure and dynamic events. The application of IMS⁶ combined with MS provides opportunities to separate gaseous protein ions based on their collision cross sections (CCSs). It can be regarded as a complement to the MS since it offers another dimensional ion separation in terms of the ion shape.

In **Chapter 2**, we examined a commercially available IMS device which is commonly used in many laboratories. TWIMS shares the similar principle of mobility separation as DTIMS. The primary difference lies in the application of a periodic electric field that provides a wave-shape propagation. This developed electric field results in the nonlinear relationship between the drift time and CCS. In order to extract Ω values from TWIMS, a calibration have to be performed based on DTIMS Ω_{ref} values. Many protocols⁷⁻⁹ aimed at solving the problem. We reproduced the calibration experiment⁸ and got the expected results. On this basis, we simplified the

algorithmic method by ignoring the negligible effect from reduced mass and the time that ions spend from transfer ion guide to mass analyzer and we obtained the parallel results. In addition, we clarified the calibration conditions which are not addressed explicitly in the protocol⁸.

The work in **Chapter 3** was mainly focused on the dispute¹⁰⁻¹¹ of whether protein solution structures are preserved in the gas phase. The application of ESI is regarded as a *gentle* ionization source to convert solution analyte into gaseous ions. nanoESI is claimed to be an even *gentler* technique. We employed TWIMS-MS to examine the CCSs of four different proteins by using these two electrospray ionization tools. The results concluded from the experiments were expected to answer the two questions above. Ω values extracted from experiments were compared with reference values which are derived from crystal structures and the MD simulation structures. It was clearly that for some of the proteins, the solution structure can be reserved to a large extent. The two electrospray sources showed no differences in terms of *softness*.

IMS has been applied in many analytical measurement, ranging from the detection of chemical warfare agents to particle sizing¹². Its incorporation with MS is a powerful technique to provide insights into the structure of proteins in the gas phase. There are still many challenges facing to the calibration issues, the valid calculations of Ω values and the reproducibility of solution structures. Although we presented a clear explanation of a prevalent calibration method, it is not executable for all the biomolecules. For example, for very small peptides, the calibrated Ω values showed significant deviations.¹³ For larger proteins such as native-like alcohol dehydrogenase (ADH) ions, the calibration exhibited large experimental errors.⁹ It is suggested that using calibrant ions that have similar masses and mobilities to those of the analyte ions results in smaller errors. Another improvement can be achieved to calculate Ω values is the use

of a recently developed “projected superposition approximation” (PSA) algorithm.¹⁴⁻¹⁷ It is superior due to its accurate evaluation of CCS with extensive range from small peptides to large protein complexes and its timesaver.

The observation of collapse in Hb is a very interesting aspect. Similar phenomena have been detected in other experiments on different protein complexes.^{11, 18} A possible explanation is that the internal cavity of these proteins collapses when they experience collisional heating. Some attempts have been made to verify this proposal. Ferrocyanide and inositol hexaphosphate are two inorganic compounds which can bind with the two β -subunits of Hb. They sit in the entry of the central cavity, which makes them to be promising impediment from collapse inside. However, the same decrease in CCS was observed with Hb bound with ligands. It is not fair to conclude that the collapse of cavity is not a reason of decrease in Ω value since the ligands are relatively small compared to Hb, additionally, they do not fill the cavity completely. Other effects on this “collapse” were found from the instrument settings. Unfortunately, there were no consistent results being obtained which makes it more complicated. Further investigations can be done with this enigma by using of IMS or other gas phase based analytical tools.

4.2 References

1. Kelly, S. W.; Jess, T. J.; Price, N. C., *Biochim. Biophys. Acta* **2005**, *1751*, 119-139.
2. Chen, E.; Wittung-Stafshede, P.; Kliger, D. S., *J. Am. Chem. Soc.* **1999**, *121*, 3811-3817.
3. Chung, H. S.; McHale, K.; Louis, J. M.; Eaton, W. A., *Science* **2012**, *335*, 981-984.
4. Rhodes, G., *Crystallography Made Crystal Clear*. 2nd ed.; Academic Press: San Diego, 2000; p pp 29-37.
5. Mittermaier, A. K.; Kay, L. E., *Trends Biochem. Sci.* **2009**, *34*, 601-611.
6. Kemper, P. R.; Dupuis, N. F.; Bowers, M. T., *Int. J. Mass Spectrom.* **2009**, *287*, 46-57.
7. Valentine, S. J.; Counterman, A. E.; Clemmer, D. E., *J. Am. Soc. Mass Spectrom.* **1997**, *8* (9), 954-961.
8. Ruotolo, B. T.; Benesch, J. L. P.; Sandercock, A. M.; Hyung, S.-J.; Robinson, C. V., *Nat. Protocols* **2008**, *3*, 1139-1152.
9. Bush, M. F.; Hall, Z.; Giles, K.; Hoyes, J.; Robinson, C. V.; Ruotolo, B. T., *Anal. Chem.* **2010**, *82*, 9667-9565.
10. Wytttenbach, T.; Bowers, M. T., *J. Phys. Chem. B* **2011**, *115*, 12266-12275.
11. Hogan, C. J.; Ruotolo, B. T.; Robinson, C. V.; de la Mora, J. F., *J. Phys. Chem. B* **2011**, *115* (13), 3614-3621.
12. Bohrer, B. C.; Merenbloom, S. I.; Koeniger, S. L.; Hilderbrand, A. E.; Clemmer, D. E., *Annu. Rev. Anal. Chem.* **2008**, *1*, 293-327.

13. Williams, J. P.; Scrivens, J. H., *Rapid Commun. Mass Spectrom.* **2008**, 22 (2), 187-196.
14. Bleiholder, C.; Wyttenbach, T.; Bowers, M. T., *Int. J. Mass Spectrom.* **2011**, 308 (1), 1-10.
15. Bleiholder, C.; Contreras, S.; Do, T. D.; Bowers, M. T., *Int. J. Mass Spectrom.* **2013**, 345, 89-96.
16. Anderson, S. E.; Bleiholder, C.; Brocker, E. R.; Stang, P. J.; Bowers, M. T., *Int. J. Mass Spectrom.* **2012**, 330, 78-84.
17. Bleiholder, C.; Contreras, S.; Bowers, M. T., *Int. J. Mass Spectrom.* **2013**, 354, 275-280.
18. Hall, Z.; Politis, A.; Bush, M. F.; Smith, L. J.; Robinson, C. V., *J. Am. Chem. Soc.* **2012**, 134, 3429-3438.

Curriculum Vitae

Yu Sun

Education

University of Western Ontario (2013 - 2015)

M.Sc. in Analytical Chemistry

Thesis title: Using Ion Mobility Spectrometry to Study Protein Conformations in the Gas Phase

Supervisor: Dr. Lars Konermann

Sichuan University, China (2009 - 2013)

B.Sc in Chemistry

Publications

Sun Y, Vahidi S, Sowole MA, McAllister RG, and Konermann L (2015) Protein Structural Studies by Traveling Wave Ion Mobility Spectrometry: A Critical Look at Calibration, Electrospray Sources, and Molecular Dynamics Models. *Analyst*. (Submitted)

Jun Yao, **Yu Sun**, Mei Yang and Yixiang Duan. (2012). Chemistry, physics and biology of graphene-based nanomaterials: new horizons for sensing, imaging and medicine. *J. Mater. Chem.*, 22, 14313

Presentations

31th Annual Trent Conference on Mass Spectrometry – August 2014

“Softness and calibration issues in travelling wave ion mobility spectrometry” **Yu Sun**, Siavash Vahidi, Lars Konermann